2021-05-01

3D Printing Of High Viscosity Fluids And Its Application In 3D Printing Of Prosthetic Teeth.

Abhilash Aditya
University of Texas at El Paso

3D PRINTING OF HIGH VISCOSITY FLUIDS AND ITS APPLICATION IN 3D PRINTING OF PROSTHETIC TEETH.

ABHILASH ADITYA

Doctoral Program in Materials Science and Engineering

APPROVED:

Namsoo Peter Kim, Ph.D., Chair

Devesh Misra, Ph.D.

Guikuan Yue, Ph.D.

David Espalin, Ph.D.

Rajkumar Lakshmanaswamy, Ph.D.

Stephen L. Crites, Jr., Ph.D.
Dean of the Graduate School

Dedication

For my parents Shamala and Venkatesha

3D PRINTING OF HIGH VISCOSITY FLUIDS AND ITS APPLICATION IN 3D PRINTING OF PROSTHETIC TEETH.

by

ABHILASH ADITYA, M.S in Mfg. Eng

DISSERTATION

Presented to the Faculty of the Graduate School of

The University of Texas at El Paso

in Partial Fulfillment

of the Requirements

for the Degree of

DOCTOR OF PHILOSOPHY

Materials Science and Engineering

THE UNIVERSITY OF TEXAS AT EL PASO

May 2021

Acknowledgments

I would first like to thank my advisor Dr. Namsoo (Peter) Kim, who expertly guided me through my graduate education. His unwavering enthusiasm for innovation kept me motivated and engaged with my research. His indulgence in building his own 3D printers sparked my interest. It made me pursue a graduate certificate in 3D engineering and additive manufacturing. Here is where I was acquainted with Dr. David Espalin, whose teachings were invaluable, and I know that I will put this knowledge to good use throughout my career. I would also like to thank Dr. Devesh Misra for his remarkable support and genuine concern throughout my time at school. My involvement in the Indian Student Association at UTEP brought me close to Dr. Rajkumar Lakshmanaswamy, whose involvement and generosity immensely benefited the association. Though the pandemic had drastically disrupted academic proceedings, Dr. Guikuan Yue went out of his way to help me with my research endeavors. For that, I express my profound gratitude.

I like to extend my appreciation to Ji Hye Kim for her artwork and her help in remote 3D printing. This research would not have been completed without their state of art 3D printing facilities at The University of Texas at El Paso and Korea University.

I also acknowledge with a deep sense of reverence my gratitude to my parents and family members, who always supported me morally and economically.

Finally, gratitude goes to all of my friends who directly or indirectly helped me throughout my graduate studies.

Any omission in this brief acknowledgment does not mean a lack of gratitude.

Abstract

The advancement in technology has brought forward non-conventional manufacturing methods that are efficient and advantageous for specific applications. 3D printing is one such outcome, whose applications stretch from biomedical applications to daily products. 3D printing is a rapidly growing technology, and innovative research developments have proven versatility in creating physical objects. Simplification and constant improvement in Fused Deposition Modeling (FDM) operation result from decades of research. However, 3D printing is material-specific and contributes to shortcomings in the technology. The build-material dictates the extrusion parameters, including the material discharge rate and head speed for a continuous flow. Customization being the prime focus of this research, demands precise control of material flow. The current study emphasizes the research involved in attaining constant material flow by applying the Hagen-Poiseuille equation for a constant discharge of non-Newtonian-high viscous fluids through a piston-type extruder. The precise control over discharge rate is achieved by controlling the tip (nozzle) size, head speed, and the pressure applied to the piston. Integration of the Internet of Things (IoT) enabled long-distance 3D printing between two continents, successfully printing Single Line Designs (SLD) and 3D structures. A similar principle is applied to the printing of human prosthetic teeth using hydroxyapatite as a potential replacement for the traditional titanium screws.

Table of Contents

List of Tables

List of Figures

+

Chapter 1: Introduction

Additive manufacturing (AM) process using Fused Filament Fabrication (FFF) or Fused Deposition Modeling (FDM), in other words, Material Extrusion (ME) employs a nozzle to extrude the build material layer over layer to create a physical object. Computer-Aided Designing (CAD) software help create a digital design and save it as STL (Standard Tessellation Language) file for 3-dimensional (3D) printers to interpret and fabricate. The advantages, such as reduced material wastage, enable extensive product customization yet create complex structures with ease and comparatively lower operating cost, making it desirable for fabricating objects that otherwise undergo conventional manufacturing techniques. It is often the material that dictates the type of AM technology used for manufacturing. The material extrusion process is usually related to the 3D printing of polymers involving the change of state from solid to a liquid by applying heat. On observation, it can be assumed that the build material at some point of the manufacturing process attains a liquid state. However, there are limited applications where the build material starts in a liquid state, and liquid extrusion is needed. This dissertation focuses on printing high viscous fluids using the material extrusion method and demonstrates some of its unique applications, including 3D printing of human prosthetic teeth.

1.1 Problem Statement

Material extrusion 3D printing is often associated with the printing of polymers, usually in solid-state in the form of a filament. Advancements in 3D printers have sought out unprecedented applications of printing ceramics and food, including telemedicine. Such applications demand a 3D printer, the capability of extruding high viscous fluids. In addition to extracting, precise material discharge is crucial for a fine print. Considering the applications such as printing small

ceramic structures, food, and telemedicine, the control over the material discharge plays a prominent role. A simple, efficient, and cost-effective material extrusion method is imperative for an accurate 3D printing operation.

3D printing technology is known for its versatility of customization, and new applications of such innovations are yet to be realized. Lately, 3D printers are moving towards high-volume production rather than individual customization. Complex design and printing mechanisms increase the cost of 3D printers. Customization plays a prominent role in food and telemedicine, and capable and cost-effective 3D printing machines are requisite.

3D printing of ceramics and food requires a unique approach to develop a simple material extrusion mechanism. The data necessary for developing such an extrusion mechanism is not readily available, and extensive experimentation is necessary. Besides, the physical attributes of viscous materials contribute to the inaccurate quantity of material extrusion at every start and stopping point, thereby increasing the print duration and structural inaccuracies in some instances.

Teeth are susceptible to damage due to injury or poor hygiene, eventually leading to the replacement of damaged teeth. Such procedures generally involve titanium implants screwed into the jawbone. However, the replaced tooth cannot recreate the sensation of the natural tooth due to the lack of the living cells (pulp) inside. Research on 3D printing of human prosthetic teeth as a potential replacement for traditional teeth implants is needed.

1.2 LITERATURE REVIEW

1.2.1 Additive manufacturing

The additive manufacturing process has constantly been evolving since the 1980s, and its spectrum of applications spans from architecture, medicine to art on the other end.[1] Advancement in 3D printing research has improved printing efficiency, speed, and performance. According to a

report from Arizton Advisory & Intelligence, the revenue from the 3D printing industry is projected to 29 billion by 2025.[2]

The additive manufacturing process is classified as follows by the American Society for Testing and Materials (ASTM).[3]

Binder jetting, additive manufacturing process in which a liquid bonding agent is selectively deposited to join powder materials.

Directed energy deposition, additive manufacturing process in which focused thermal energy is used to fuse materials by melting as they are being deposited.

Material extrusion, additive manufacturing process in which material is selectively dispensed through a nozzle or orifice.

Material jetting, additive manufacturing process in which droplets of build material are selectively deposited.

Powder bed fusion, additive manufacturing process in which thermal energy selectively fuses regions of a powder bed.

Sheet lamination, additive manufacturing process in which sheets of material are bonded to form a part.

Vat photopolymerization, additive manufacturing process in which liquid photopolymer in a vat is selectively cured by light-activated polymerization.

Of all the AM processes, material extrusion is widely used due to its lower cost and ease of operation. Solidworks, CATIA, and Autodesk are a few Computer-Aided Designing (CAD) software that helps create digital designs in STL files. The digital designs are directly used as an input to print a three-dimensional object. This process of design input is typical for all the AM processes. However, the preprocessing of material involved in 3D printing and the post-processing

of the 3D printed parts differ from one Am process to another. Non-conventional manufacturing methods such as AM have been improving since it was introduced three decades ago and can now print metals, ceramics, and polymers.[4,5,6]

1.2.2 Material extrusion

According to ASTM, "material extrusion is an additive manufacturing process in which material is selectively dispensed through a nozzle or orifice."[3] (Figure 1.1)It is the most popular AM process due to its cost and accessibility. This AM process builds a three-dimensional object on a platform by depositing molten polymer.[7] It is also referred to as Fused deposition modeling (FDM), and it holds the largest market share of polymer AM processes.[8] Due to the original patient's expiration on the technology in 2009, do-it-yourself (DIY) kits were released, and the popularity has been growing ever since.[9] The major drawback of this process is the dependence on amorphous polymeric materials as a feedstock and the lack of compatible printable material other than acrylonitrile butadiene styrene (ABS)and polylactic acid (PLA).[10]

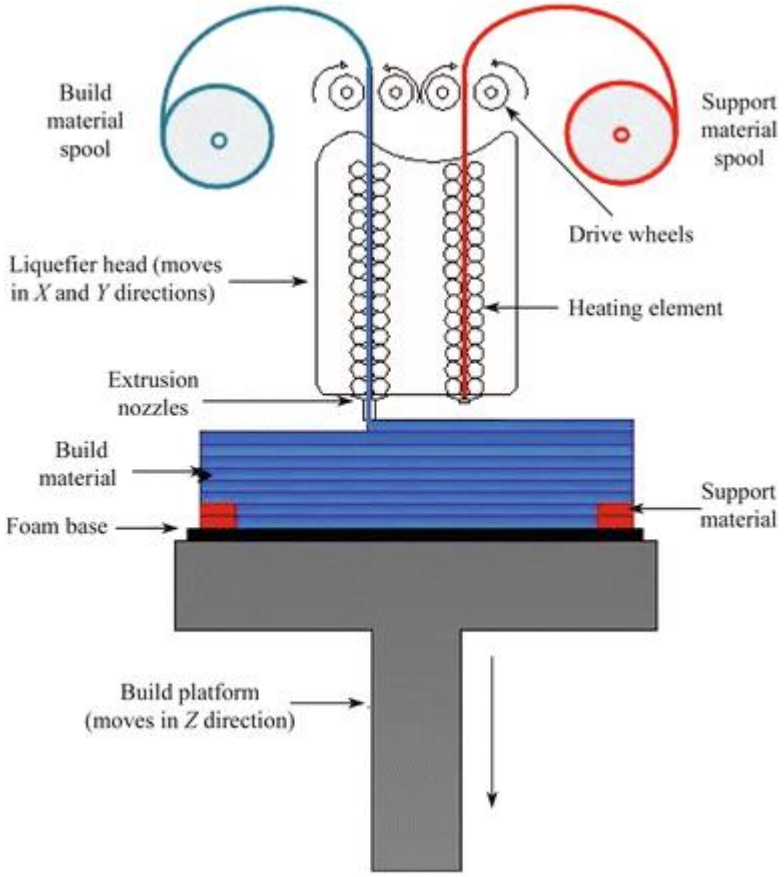

Figure 1.1: Schematic diagram of material extrusion AM process with build and support material spools.[11]

Improvising the technology has been sought after due to the popularity of the AM process. Researchers have made an effort to investigate the effect of process parameters on dimensional accuracy, tolerance control, build time, mechanical properties, and surface roughness.[12,13,14,15,16] Extensive research on design methods is studied and discussed for improving the quality of polymer 3D printing.[17]

1.2.3 Rheology of fluids

A branch of physics studying the deformation and flow of matter is referred to as 'rheology,' and the Professor Bingham of Lafayette College coined the term.[18] Newtonian fluids and non-Newtonian fluids are standard terms while discussing the rheology of fluids. Fluids used

in daily life, such as water, paint, peanut butter, ketchup, etc., have different consistencies and flow differently. The type of flow is often based on the relationship between the shear stress (τ) and the strain rate ($\frac{dV}{dy}$). (V - average velocity; μ - absolute viscosity.) The relationship changes according to the fluid and it is as explained in the Figure 1.2 (A) and (B).

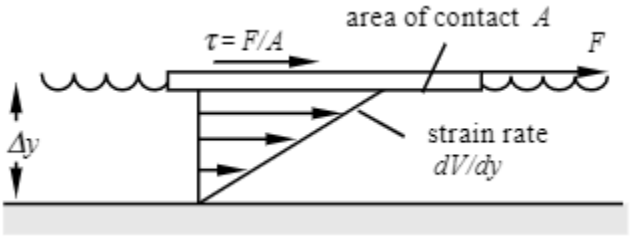

Figure 1.2 (A): Shear stress applied to a liquid[19]

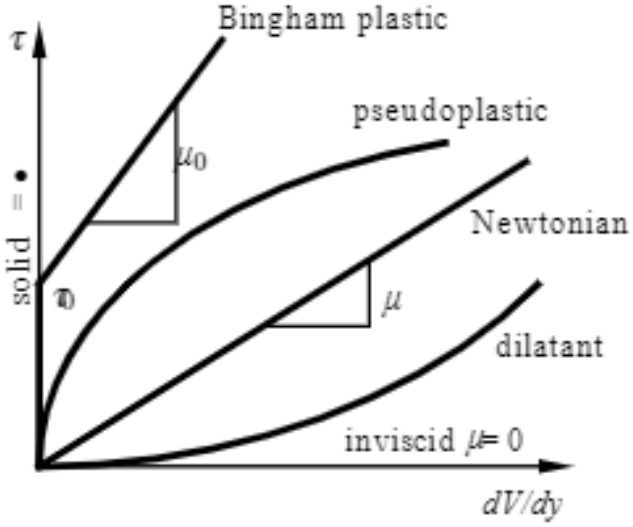

Figure 1.2 (B): Relationship between the shear stress and strain rate of various fluids.[19]

Newtonian fluids exhibit a linear relationship with shear stress and the strain rate, as seen above. In comparison, all other fluids except Bingham plastic exhibit a non-linear relationship. Bingham plastics need higher shear stress before they start flowing linearly.

Newtonian fluids expression by newton's law of viscosity, considering shear stress (τ) and shear rate (γ), is shown below.[20,21]

$$\tau = -\mu\gamma$$

(μ- Coefficient of dynamic viscosity)

Non- Newtonian fluids can be broadly classified into the following 3 classes based on the shear stress and shear rate.[22]

- Time independent non-Newtonian fluids

  The shear rate has a unique but non-linear function of instantaneous shear stress.

  $$\gamma=f(\tau)$$

  Bingham plastics, pseudoplastic and dilatant fluids exhibit such behavior.

- Time-dependent non-Newtonian fluids

  The relationship between shear stress and shear rate is complex as the shear also depends on shearing time or previous shear rate history. Depending on the increase or decrease of shear stress, the materials are classified as thixotropic and rheopectic fluids. (Figure 1.3)

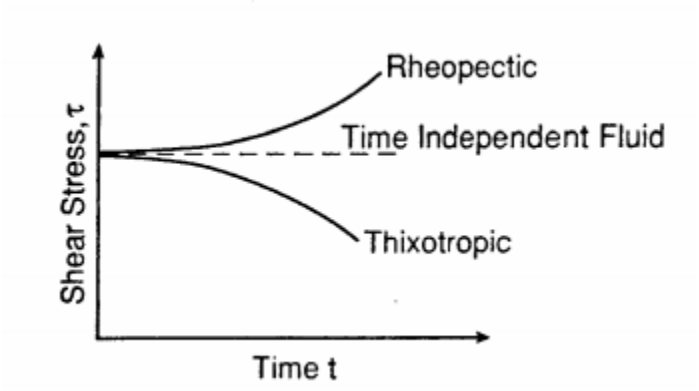

Figure 1.3: Behavior of time-dependent non-Newtonian fluids with shear stress.

- Viscoelastic non-Newtonian fluids.

  The fluid exhibits both viscous and elastic properties. The rheological property is the relationship between shear stress and shear rate, including time derivatives of both quantities.

$$\tau = \frac{d\gamma}{dt} - \frac{\mu}{\lambda}\frac{d\tau}{dt}$$

(μ-Viscosity; λ-Rigidity modulus)

The experimentation on 3D printing with polymers using material extrusion has proved that the material's viscosity should be of toothpaste consistency (70000 - 100000cP) for effective printing. Most 3D material extrusion techniques deal with solid materials at room temperature and have to be melted for the 3D printing process.

1.2.4 Hagen-Poiseuille (HP) equation

The equation was independently put forward by Jean Léonard Marie Poiseuille and Gotthilf Heinrich Ludwig Hage

n and was published in 1846.[23,24] The theoretical justification of the equation was given by George Stokes in 1845.[25] Hagen- Poiseuille equation establishes the relationship between the flow rate (Q) and the pressure gradient (ΔP) across the length of the cylinder (L) with a certain radius (R) and fluid viscosity (μ).[26]

$$Q = \frac{\pi R^4 \Delta P}{8\mu L}$$

The steady laminar fluid flow of an incompressible Newtonian fluid in a long rigid cylindrical pipe exhibits a parabolic profile due to the velocity of flow ranging from zero at the walls to reaching maximum velocity at the centerline.[27] (Figure 1.4)

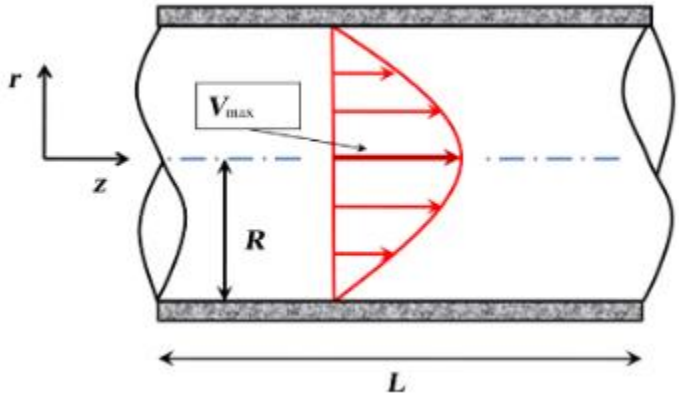

Figure 1.4: Parabolic profile of a laminar fluid flow of a Newtonian fluid.[27]

The equation is used to quantify the fluid flow of Newtonian fluids, including air, essential for medical applications involving hypodermic injections and respiratory care.[28,29] The equations can also be applied to microfluidics dealing with biological and chemical experimentation involving microchannels measurements ranging from nano to microliters (10^{-9}- 10^{-6} L) or smaller.[30] The equation is essential for experimentations dealing with fluid flow inside a cylindrical tube.

1.2.5 Material Extruders

A material extruder is the most crucial part of an AM process, such as material extrusion. The material extruder contains the build material until the extrusion process is initiated. It then extrudes the required amount onto the print platform layer-by-layer to form a three-dimensional object. The extruder in the polymer material extrusion AM process houses a heater to melt the filament, and the motors behind the extruder push the filament further to supply fresh solid filament and push out the molten filament. The schematic diagram of a filament extruder is shown in Figure 1.5, illustrating the components involved in the process of extrusion.

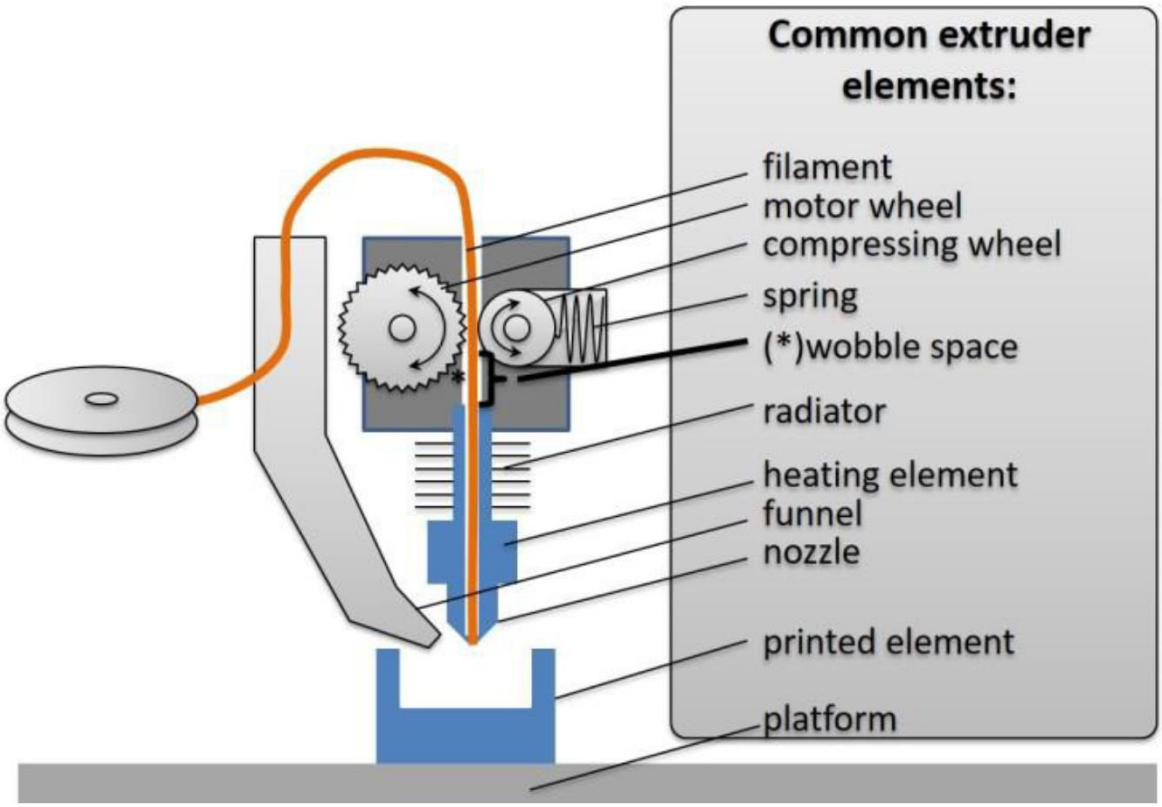

Figure 1.5: Schematic diagram of an extruder in a material extrusion AM process.[31]

Unprecedented applications of 3D printers in the food and pharmaceutical industries emerged, forcing the innovation of the material extrusion process to print materials that are not solid at room temperature. Food and ceramic 3D printing is an emerging industry, and innovative research efforts on efficient food painting resulted in position-type and screw-type extruders.[32,33] An extruder mechanism must control the quantity of fluid discharge from the nozzle. Few of such ambitious extrusion mechanisms were put forth to print fluid, and the gap between the available functionalities and the consumer needs is elaborately discussed.[34] (Figure 1.6)

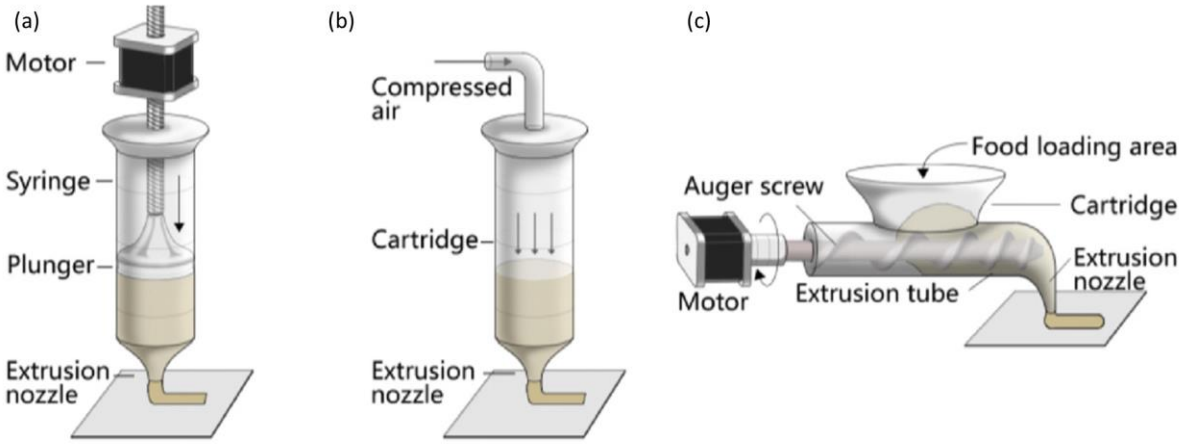

Figure 1.6: (a) Syringe-based extrusion; (b) Air pressure-driven extruder; (c) Screw-based extrusion[34]

The operating mechanism of an extruder for material discharge has been steadily improving. However, precise control over the material discharge is still questionable considering pharmaceutical applications. The inherent property of the non-Newtonian fluids makes it challenging to control the exact moment of discharge in the beginning and the bleed effect when the extruder stops.

1.2.6 Internet of Things (IoT)

As Kevin Ashton claimed, the phrase 'Internet of things' was first used in a presentation about Radio-Frequency Identification (RFID) in the P&G supply chain in 1999.[35] IoT is described as "the networked interconnection of everyday objects, which are often equipped with ubiquitous intelligence."[36] IoT has gained massive importance in recent years in modern wireless telecommunication. IoT is the convergence of things, the internet, and semantic-oriented vision, as shown in Figure 1.7.

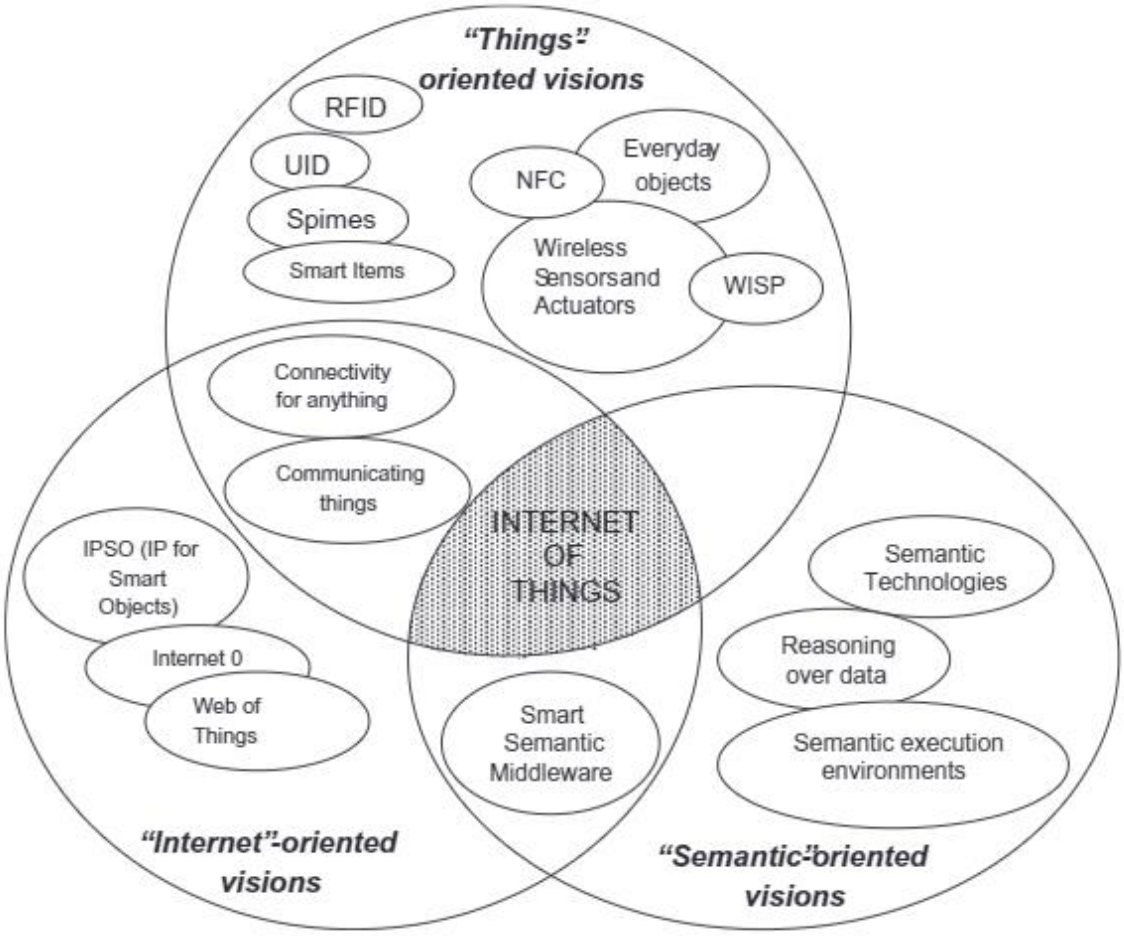

Figure 1.7: Internet of things as a convergence of different visions.[37]

The potential of IoT is far-reaching and is grouped into the following domains and illustrated in Figure 1.8.[37]

- Transportation and logistics domain.
- Healthcare domain.
- Smart environment (home, office, plant) domain.
- Personal and social domain.

Figure 1.8: Potential application domains of IoT.[37]

Since the introduction of IoT, the development in the field has seen a signifi

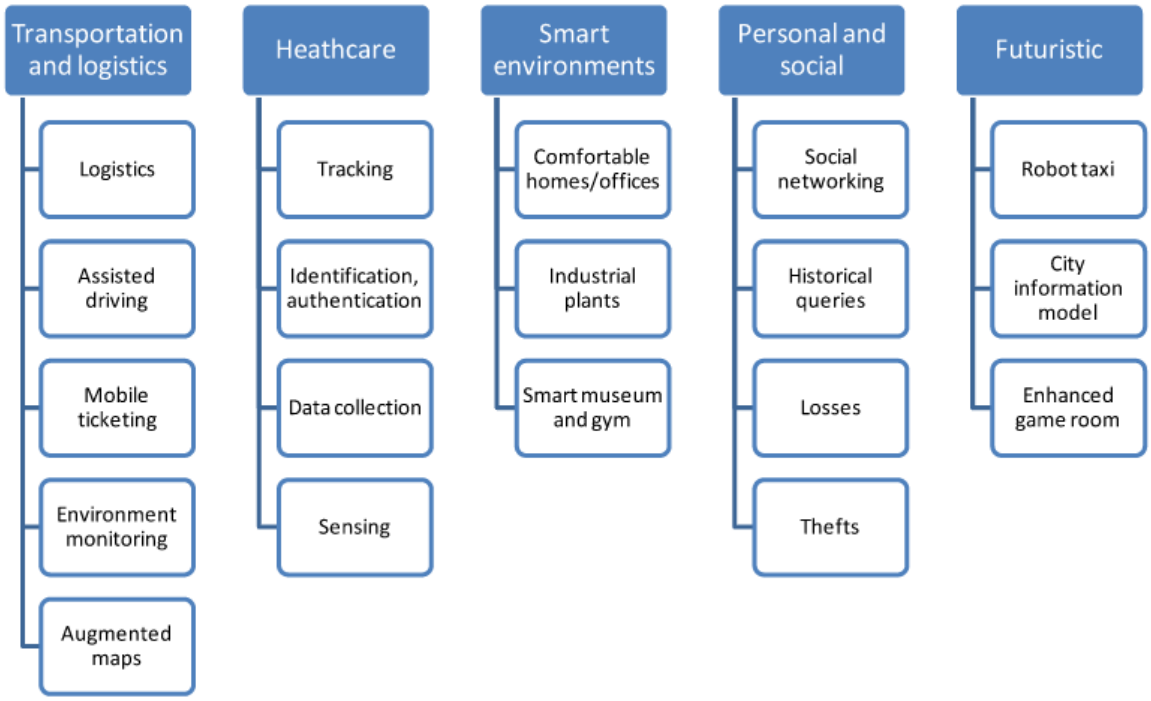

cant rise in its applications, and constant research has the technology seep through other walks of life. Figure 1.9 shows the exponential evolution and progress of IoT since it was introduced at the beginning of the 2000s.

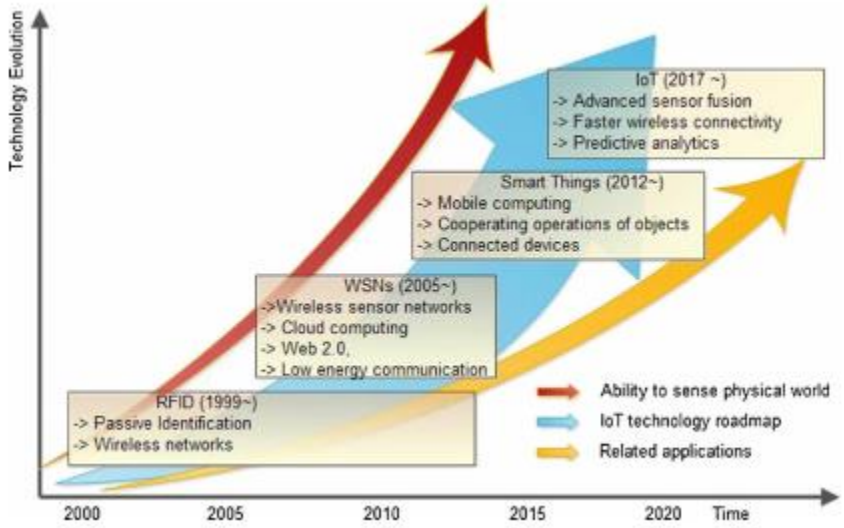

Figure 1.9: Evolution of the IoT.[38]

1.2.7 Background of teeth and their impact on life

Most of the vertebrates exhibit the ability of tooth regeneration. Most mammals regenerate teeth once (diphyodonty) than other species such as reptiles regenerating teeth multiple times (polyphyodonty).[39,40] Oral injuries are frequent, and trauma to the oral region comprises 5% of all injuries in which 18% of all somatic injuries are oral in the age group of 0-6 years, making it the second most common injury.[41] In addition to trauma, chronic diseases, tobacco, alcohol, unhealthy diet, and lack of physical activity may lead to oral complications.[42]

In research conducted using education as a socioeconomic position, the USA displayed significant disparities in edentulism.[43] Adults with less than 20 teeth undergo psychological stress, and income inequality can be related to tooth loss.[44,45] Thus, damaged teeth or lack of teeth may cause social or psychological discomfort in humans. For one's wellbeing, a presumption is that the replacement of damaged teeth is essential. According to recent studies, one out of four teeth replantations showed functional recovery, indicating the necessity for researching procedures for tooth regeneration (periodontal ligament, PDL in specific) after tooth avulsion.[46]

1.2.8 Dental implants and materials

Numerous proposals of alternatives for teeth replacement/replantation, of which few have shown success in recent years. The use of stem cells to regenerate tooth is one of the fanciest research put forth with numerous drawbacks with the lack of control over the size, shape, and color of teeth.[47] Evidence shows bioengineered tooth holds the potential solution for tooth replacement, displaying successful replantation on mice.[48] History points the practice of teeth transplantation back to centuries.[49]

A dental implant is a surgical orthodontic anchor interfacing the jaw's bone or the skull to support dental prosthetics.[50] (Figure 1.10) Endosteal and subperiosteal are the broad classifications

of dental implants. Endosteal implants take the support of the bone, whereas the subperiosteal implants rest on the bone under the periosteum.[51] The fabrication of dental implants utilizes all three classes of materials, such as metals, ceramics, and polymers, as few of them process physical and chemical properties such as adequate strength, toughness, wear, fracture, and corrosion resistance along with biocompatibility.[52] The use of metals and their biocompatibility, especially titanium, for biomedical implants was prominent since 1940.[53,54]

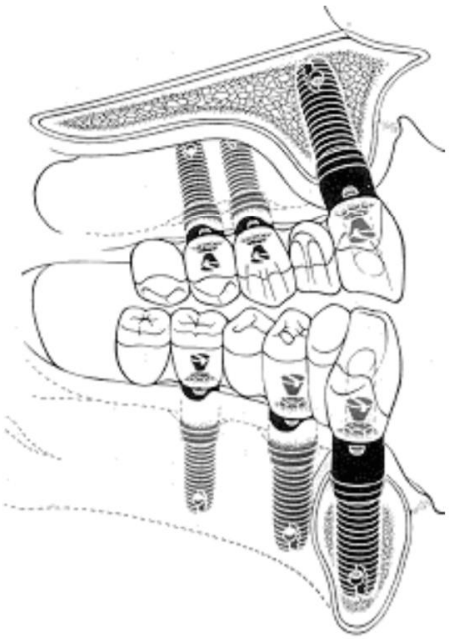

Figure 1.10: Osseointegrated screw is inserted in the edentulous mandible.[55]

Research over the years bolsters the essence of biocompatibility of titanium alloys.[56,57] Recent studies indicate Binary Titanium alloys (<20%) with Zirconium (Zr), Indium (In), Silver (Ag). Copper (Cu), Gold (Au), Palladium (Pd), Niobium (Nb), Manganese (Mn), Chromium (Cr), Molybdenum (Mo), Tin (Sn), Cobalt (Co), Germanium (Ge), and Gallium (Ga) exhibit better mechanical and potential biocompatibility compared to pure titanium (cp-Ti).[58] Having seen the benefits, titanium dental implants have gained popularity and are widely used in recent years.

Though titanium stands as an ideal material for dental implants, it has few drawbacks, creating a necessity to bring about new alternatives to replace the existing procedures.

Titanium is biocompatible; however, the rate of osseointegration is low as surface roughness plays a vital role in cell proliferation on the surface of the implant.[59] The traditional manufacturing process of titanium dental implants fails to provide necessary surface roughness, rectified by post-processing methods such as Titanium Plasma Sprays (TPS), Sandblasting, Acid-Etching, and SLA (the process involves both sandblasting and acid-etching).[60,61] Metal hypersensitivity persists in people with a history of allergy to metals, creating a sequence of undesirable reactions by the immune system resulting in no safe limit or acceptable metal level in the body.[62,63,64,65] Considering the drawbacks of using metal as an implant, it is safe to move to a material that the body is familiar with and accepts.

Hydroxyapatite, β-tricalcium phosphate, in other words, is a bioceramic material known for its osteoconductive and osteoinductive properties.[66,67] Studies have substantiated the improvement of the performance of titanium implants after coating with such material.[68] The use of hydroxyapatite for bone substitute or bone grafting can be dated back to 1920.[69] This type of bioceramic has developed as research progressed over the years. A review of several pieces of literature on such bioceramics illustrates the high potential of using such material in biomedical implants.[70]

1.2.9 Evolution of dental manufacturing processes.

The manufacturing process for dental implants has evolved over the centuries, depending on the available material and technology at the corresponding periods. Dental implants have come a long way from black stone implants in Mayan mandible shells, the use of animal teeth, and

different metals until the currently bioengineered dental implants.[71] Casting and milling are some of the conventional manufacturing processes for dental implants.[72,73] These traditional manufacturing processes come with their share of limitations, such as pipping defect in casting[74] and wastage of raw materials in milling as it is one of the subtractive manufacturing processes. The recycling process can reduce wastage of the raw materials[75], but the recycling process, in turn, increases the cost of production.

Thus, the need to improve biocompatibility and rectify the existing drawbacks of traditional manufacturing processes began the additive manufacturing process. The possibilities in improving dental implants grew as 3D modeling, and additive manufacturing could increase porosity, surface roughness, and rapid osteointegration.[76,77] Manufacturing metallic dental implants using the additive manufacturing processes utilize laser or electron beam, resulting in all the desired properties.[78] Having considered the drawbacks of metallic implants, hydroxyapatite in additive manufacturing for dental implants was essential. The incorporation of binder jetting is appropriate for 3D printing of hydroxyapatite, and such a process can achieve the desired properties for a dental implant.[79,80,81]

Manufacturing processes allowing the possibility of controlling the porosity of bone implants capable of osteointegration are by gel casting and polymer sponge method resulting in a porous structure.[82] The foam gel technique (use of polymers), by virtue, possesses the potential of being an innovative manufacturing process in tissue engineering.[83,84] This innovative method of creating porosity is suitable for creating implants that are essential for cell proliferation.

1.2.9 Bioengineered teeth

Replacement of damaged or loss of teeth by bioengineered teeth is not unheard of in recent years. The latest stem cell research shows promising possibilities in regenerative medicine, where teeth can be grown to replace the damaged or missing teeth.[85] Developing porous hydroxyapatite scaffolds capable of sustaining and aid cell proliferation is studied using stem cells.[86,87] The study of stem cells' characterization provides insight on the properties depending on tissue source and plays a vital role in bioengineered organs.[88] Dental pulp stem cells (DPSC) share similarities with bone marrow stem cells (BMSC) capable of assisting de novo pulp regeneration suitable for bioengineered teeth.[89] Furthermore, DPSCs are multipotent, where they can differentiate into numerous cell lineages depending on the necessity of functional regenerative requirements.[90] Several successful research indicates the potential of various 3D printing technologies for printing dental implants and the use of stem cells for regenerative dental applications.[91]

Chapter 2: Process parameters in 3D printing

2.1 3D PRINTER

The 3D printer in this study falls under the material extrusion AM process category as the material is dispensed through an orifice. Unlike other material extrusion processes, this study focuses on printing materials that are fluid at room temperature. The material feeding and dispensing mechanisms had to be designed for printing viscous fluids. It is usual for the printing parameters for the 3D printer can vary depending on the application. One of the major drawbacks of 3D printers is the range of materials a single machine can print. However, an attempt was made to calibrate the 3D printers' process parameters to print various materials without compromising the result. Customization and accessibility being the focal point of the research, the 3D printers are linked through the cloud to access design data and long-distance printing. Most 3D printers printing viscous fluids are either not precise or expensive. The printer head movement mechanism and the material extruder efficient to keep the design simple and the cost low.

A cartesian coordinate XYZ motion mechanism with 3 motors for each direction is the typical material extrusion setup. A monkey bar setup for XYZ motion of the 3D printer is used in this study. The speed at which the head moves while printing has an immense effect on the resultant product. Printing parameters such as head speed, the effect of nozzle tip size, and the pressure applied to extrude the material contribute to printing performance. The switch from filament printing to fluid printing requires changes in the extruder mechanism. Due to its inherent property, extruding viscous fluids poses challenges such as resistance to free flow unless an external force is applied. A mechanism to start and stop the flow of viscous fluids from the extruder is crucial, and this study discusses the application of an innovative Piston-Type Extruder (PTE). The data required for such an extrusion mechanism is not readily available, and repeated

experimentations were necessary. Though the study is based on high viscous fluids, the experiments were carried out using the HP equation and optimized for effective material extrusion.

2.1.1 Appearance of the 3D printers.

The 3D printers used in this study are enclosed in an aluminum casing to ensure safe 3D printing operation. The tabletop 3D printers are compact and also comes with an aluminum stand as an option. The 3D printers have an 8 in X 4 in screen to display the printing process, printing information, texts, and videos. (Figure 2.1) The aluminum casing protects the things which are printed if they are susceptible to change when exposed to an open environment.

Figure 2.1: 3D printers installed in K-CBD center Korea University, Seoul

2.1.2 The Piston-type extruder (PTE)

The material extruder is a vital part of the 3D printer as it dispenses the material on demand. The PTE is a cylindrical tube with a piston on one end and a muzzle on the other end. The fluid movement inside the cylinder exerts pressure throughout the body resulting in a pressure drop at

3 points of interest. (Figure 2.2) They are at the interface of the material and (1) the piston (ΔP_{Piston}), (2) nozzle tip(ΔP_{Tip}), and the interface between the piston and the cylinder walls ($\Delta P_{Friction}$). The nozzle tip size of the PTE can be changed according to the needs. However, for printing viscous fluids, the nozzle must be big enough for the material extrusion and small enough to prevent the material from leaking while not printing. A motor above the PTE exerts pressure on the piston translating rotatory motion to linear motion. The exerted pressure on the piston pushes the piston downwards, extruding the material out of the nozzle and onto the build platform.

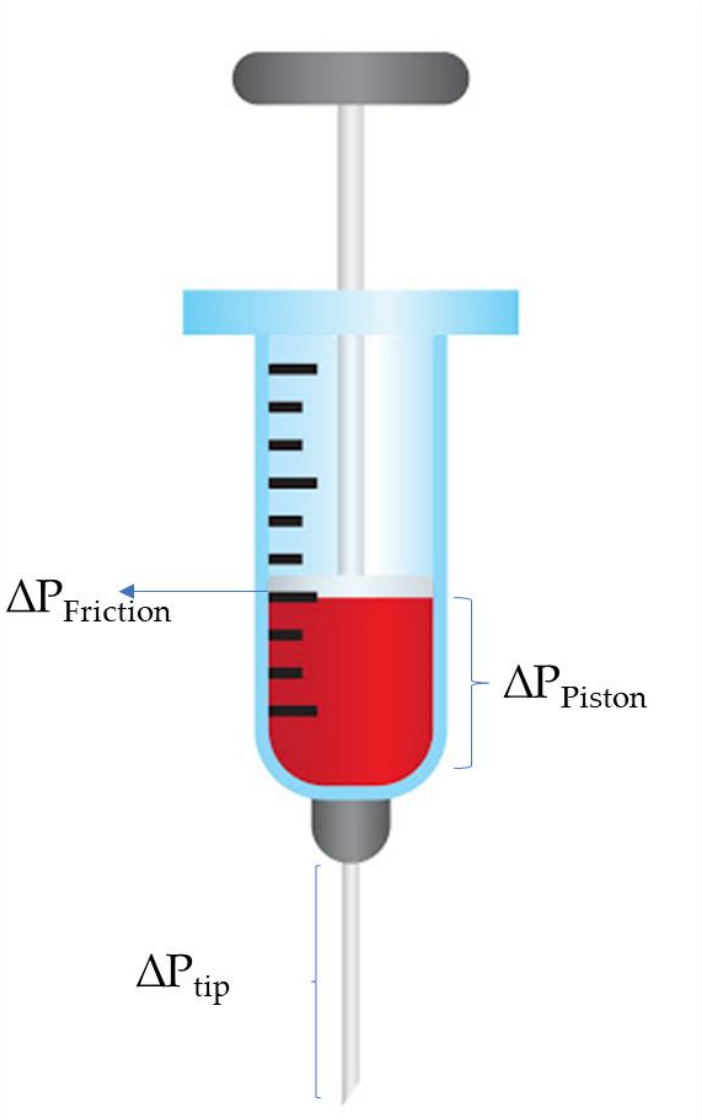

Figure 2.2: Schematic diagram of piston-type extruder (PTE) with pressure drop.

2.1.3 Internet of Things (IoT) integration

The 3D printers in this study are IoT integrated and equipped with Raspberry Pi for encrypted web access and Arduino for onboard control. Arduino is an open-source hardware and software component, a microcontroller kit that controls onboard functions such as XYZ movement and operation of the extruder. (Figure 2.3 Left) The 3D printer has onboard pressure and weight sensors to record and monitor pressure applied accurately with the help of Arduino. (Figure 2.3 Right) Recording accurate data was crucial for the research to optimize the printing parameters for efficient viscous fluid printing. Raspberry Pi is an onboard computer for accessing the web for design data input and media to display on the screen. The interaction of the 3D printer through the web to access information is a step towards IoT. However, the onboard computer can only receive data. The pandemic of COVID19 has shown the importance of non-face to face or 'untact' method of service industries. IoT integrated 3D printers can be a good fit for service industries as it requires minimal human interaction.

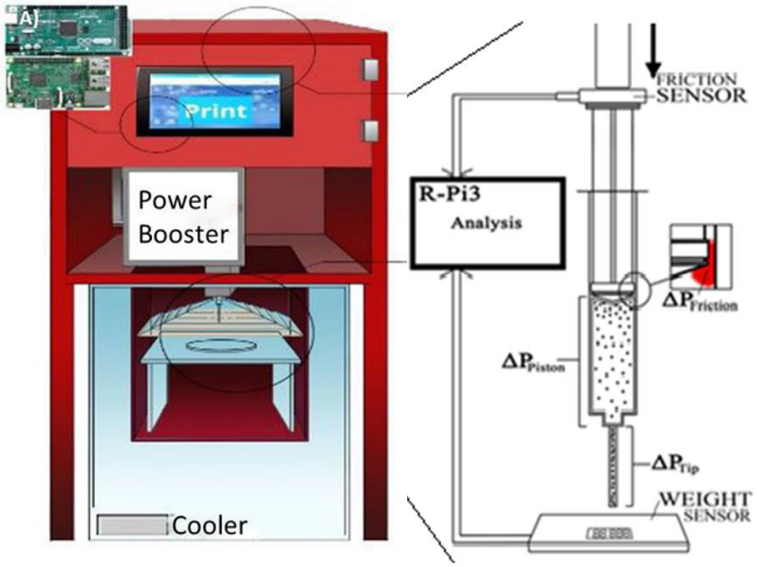

Figure 2.3: Left: Raspberry Pi and Audrino integrated, and IoT enabled 3D printer. Right: Schematic diagram of onboard sensors.

2.2 PRELIMINARY DATA COLLECTION

2.2.1 Preliminary experimental setup

3D printing of materials that are fluid with considerable viscosity at room temperature is an emerging field, and there is no readily available data to proceed. Though there are 3D printers capable of printing high viscous fluids, the data on quantitative material discharge is vague. The amount of pressure applied for material extrusion, print parameters such as head speed and nozzle tip size need to be optimized for better printing performance. The Arduino hardware and software-assisted 3D printers help monitor the data acquired from the pressure and weight sensors in real-time. The acquired arbitrary data is analyzed using the HP equation to optimize the process parameters.

Newtonian fluids such as air and water are used to obtain initial data. The experiment was carried out with hemp oil to examine the variation in their behavior. Audrino has programmed to convert the applied pressure of the total applied force into pressure applied across the cross-sectional area of the piston. The pressure applied on the top of the piston and the distance moved to reach the standard position are measured and analyzed simultaneously through sensors. The data from the experiments contain the quantity of material deposited and the pressure applied on to the piston. Repeated experimentation can provide sufficient data to check which pressure drop had a significant effect on the process. Such data is valuable to precisely control quantitative discharge from the extruder by applying appropriate pressure on the piston. Table 2.1 provides information on the minimum and maximum pressure applied from the sensor, simulated and calculated shear rate and linear velocity data, along with dynamic viscosity and density of the fluids. The experiment used the nozzle tip size r_{Tip} of 7.5×10^{-5} m to1.0×10^{-3} m at various velocities of presses

from 8.3×10^{-5}m/s to 3.3×10^{-3} m/s. The experiment was repeated up to 5-15 times to converge to 95% of the total significance level.

Table 2.1: Applied force, shear rate, and velocity of press data used in the experiment.

	Dynamic Viscosity (Pa·s)	Density (g/m^3)	Applied Force (N)		Shear rate ($/s^{-1}$)		Velocity of press (m/s)	
			Min.	Max.	Min.	Max.	Min.	Max.
Air	1.81E-05	1.23E-03	2.41E+00	7.96E+00	1.90E+01	5.33E+05	8.33E-05	1.67E-03
Water	8.90E-04	9.97E-01	8.20E-01	1.16E+01	1.92E+01	8.59E+04	8.33E-05	1.67E-03
Oil	3.0E-02	8.83E-04	1.11E+00	1.40E+02	1.90E+01	8.61E+04	8.33E-05	1.67E-03

The data obtained from the experiment is calculated by using a modified HP equation, as shown below.

$$q_v = \frac{\pi r^4 \Delta P}{8\mu L}$$

q_v: Volumetric flow rate (m^3/s)

r: Internal radius of the tube (m)

ΔP: Pressure difference between the two ends (Pa),

μ: Dynamic fluid viscosity (Pa. s)

L: Length of the tube (m)

The mass flow rate or mass flux (q_w) is obtained by multiplying the volumetric flow rate (q_v) with density (ρ).

$$q_w = q_v \times \rho$$

ρ: Density of materials (g/m^3)

Therefore,

$$q_w = \frac{\pi r^4 \Delta P \rho}{8\mu L}$$

This equation is rearranged to calculate individual pressure drops such as ΔP_{Piston} and $\Delta P_{Tip,}$ as shown below.

$$\Delta P_{Piston} = \frac{8\mu(L_{Piston})q_w}{\pi\rho(r_{Piston})^4}$$

$$\Delta P_{Tip} = \frac{8\mu(L_{Tip})q_w}{\pi\rho(r_{Tip})^4}$$

r_{Piston}: The internal radius of the piston (m)

r_{Tip}: The internal radius of the tip (m)

L_{Piston}: The length of the piston (m)

L_{Tip}: The length of the tip (m)

The total pressure drop needed to extrude the material is the sum of individual pressure drops.

$$\Delta P_{Total} = \Delta P_{Friction} + \Delta P_{Piston} + \Delta P_{Tip}$$

Hence,

$$\Delta P_{Total} = \Delta P_{Friction} + \frac{8\mu(L_{Piston})q_w}{\pi\rho(r_{Piston})^4} + \frac{8\mu(L_{Tip})q_w}{\pi\rho(r_{Tip})^4}$$

The linear velocity of extruded materials (v_z) and shear rate (γ) is calculated as shown below.

$$v_z = \frac{q_v}{\pi(r_{Tip})^2}$$

$$\gamma = \frac{4v_z}{r_{Tip}}$$

v_z: Linear velocity of extruded materials (m/s)

γ: Shear rate (1/s)

2.2.2 Preliminary results

The data from the sensors is calculated and tabulated in Table 2.2.

Table 2.2: Calculated data of all pressure drop, shear rate, and volumetric flow rate along with the recorded data of velocity of press over different nozzle tip sizes.

	Velocity of Press (m/s)	Tip size (m)	Shear Rate (s^{-1})	$\Delta P_{Friction}$ (Pa)	STDEV of $\Delta P_{Friction}$	ΔP_{Tip} (Pa)	STDEV of ΔP_{Tip}	$\Delta P_{Friction}$ (Pa)	q_v (m^3/s)	STDEV of q_v
Air	8.33E-05	4.00E-04	2.99E+02	2.39E+04	1.83E+03	4.06E-01	2.20E-01	1.47E-05	1.50E-08	8.16E-09
	8.33E-05	2.00E-04	2.34E+03	2.67E+04	2.32E+03	6.39E+00	2.69E+00	1.44E-05	1.47E-08	6.22E-09
	8.33E-05	1.10E-04	1.43E+04	2.88E+04	2.60E+03	7.04E+01	3.37E+01	1.45E-05	1.49E-08	7.13E-09
	8.33E-05	7.50E-05	4.49E+04	3.04E+04	1.41E+03	3.25E+02	1.49E+02	1.45E-05	1.49E-08	6.81E-09
	1.67E-04	7.50E-04	2.94E+02	4.19E+04	None	2.13E-01	None	9.47E-05	9.73E-08	None
	3.33E-04	7.50E-04	5.81E+02	3.62E+04	None	4.21E-01	None	1.88E-04	1.93E-07	None
	5.00E-04	7.50E-04	8.72E+02	2.98E+04	None	6.31E-01	None	2.81E-04	2.89E-07	None
	6.67E-04	7.50E-04	1.14E+03	1.99E+04	None	8.26E-01	None	3.68E-04	3.78E-07	None
	8.33E-04	1.00E-03	1.90E+01	1.55E+04	9.20E+02	1.03E-02	1.03E-02	1.46E-05	1.49E-08	7.40E-09
	8.33E-04	7.50E-04	4.52E+01	2.07E+04	1.41E+03	3.27E-02	1.63E-02	1.46E-05	1.50E-08	7.44E-09
	8.33E-04	1.00E-03	1.83E+02	1.44E+04	1.85E+03	9.93E-02	7.58E-03	1.40E-04	1.44E-07	1.10E-08
	8.33E-04	7.50E-04	4.32E+02	2.08E+04	1.30E+03	3.13E-01	2.32E-02	1.40E-04	1.43E-07	1.06E-08
	8.33E-04	7.50E-04	1.41E+03	1.90E+04	None	1.02E+00	None	4.56E-04	4.68E-07	None
	8.33E-04	4.00E-04	2.86E+03	2.13E+04	1.35E+03	3.88E+00	3.17E-01	1.40E-04	1.44E-07	1.17E-08
	8.33E-04	2.00E-04	2.28E+04	2.50E+04	1.58E+03	6.20E+01	4.91E+00	1.40E-04	1.44E-07	1.14E-08
	8.33E-04	1.10E-04	1.38E+05	2.90E+04	1.92E+03	6.80E+02	6.15E+01	1.40E-04	1.44E-07	1.30E-08
	1.67E-03	7.50E-04	8.58E+02	2.96E+04	1.28E+03	1.00E+00	0.00E+00	2.77E-04	2.84E-07	9.92E-09
	1.67E-03	4.00E-04	5.66E+03	2.94E+04	8.92E+02	8.00E+00	0.00E+00	2.77E-04	2.84E-07	1.01E-08
	1.67E-03	2.00E-04	4.51E+04	2.61E+04	1.40E+03	1.23E+02	4.00E+00	2.76E-04	2.83E-07	8.83E-09
	1.67E-03	1.10E-04	2.75E+05	3.41E+04	1.16E+03	1.36E+03	5.40E+01	2.80E-04	2.87E-07	1.14E-08
	3.33E-03	7.50E-04	1.67E+03	3.14E+04	5.37E+02	1.21E+00	2.76E-02	5.40E-04	5.55E-07	1.26E-08
	3.33E-03	4.00E-04	1.10E+04	3.47E+04	9.43E+02	1.49E+01	4.43E-01	5.38E-04	5.53E-07	1.64E-08
	3.33E-03	2.00E-04	8.83E+04	3.31E+04	5.14E+02	2.40E+02	5.68E+00	5.40E-04	5.55E-07	1.31E-08
	3.33E-03	1.10E-04	5.33E+05	4.49E+04	8.73E+03	2.63E+03	4.58E+01	5.42E-04	5.57E-07	9.70E-09
Water	8.33E-05	2.00E-04	2.37E+03	4.83E+03	3.10E+02	3.17E+02	1.06E+01	6.41E-04	1.49E-08	4.99E-10
	8.33E-05	4.00E-04	2.95E+02	5.76E+03	1.01E+03	1.91E+01	3.23E+00	6.36E-04	1.48E-08	2.18E-10
	8.33E-05	7.50E-04	4.56E+01	4.89E+03	4.15E+02	1.62E+00	1.15E-01	6.49E-04	1.51E-08	1.07E-09
	8.33E-05	1.00E-03	1.92E+01	6.08E+03	4.06E+02	5.13E-01	5.13E-01	6.49E-04	1.51E-08	1.05E-09
	8.33E-04	2.00E-04	2.17E+04	1.09E+04	9.20E+02	2.89E+03	1.74E+02	6.52E-03	1.37E-07	8.19E-09
	8.33E-04	4.00E-04	2.72E+03	8.19E+03	1.64E+03	1.76E+02	3.13E+01	6.54E-03	1.36E-07	7.63E-09
	8.33E-04	7.50E-04	4.13E+02	8.73E+03	8.04E+02	1.47E+01	7.41E-01	6.55E-03	1.37E-07	6.90E-09
	8.33E-04	1.00E-03	1.74E+02	8.45E+03	9.85E+02	4.64E+00	4.64E+00	6.53E-03	1.36E-07	7.83E-09
	1.67E-03	2.00E-04	4.29E+04	2.86E+04	3.16E+03	5.71E+03	5.18E+02	1.29E-02	2.70E-07	2.44E-08
	1.67E-03	4.00E-04	5.37E+03	1.16E+04	2.43E+03	3.46E+02	7.30E+01	1.29E-02	2.70E-07	2.14E-08
	1.67E-03	7.50E-04	8.17E+02	1.10E+04	8.31E+02	2.91E+01	2.18E+00	1.30E-02	2.71E-07	2.03E-08
	1.67E-03	1.00E-03	3.45E+02	1.04E+04	1.14E+03	9.22E+00	9.22E+00	1.30E-02	2.71E-07	1.92E-08
	3.33E-03	2.00E-04	8.59E+04	5.76E+04	4.54E+03	1.14E+04	9.89E+02	2.57E-02	5.40E-07	4.65E-08
	3.33E-03	4.00E-04	1.07E+04	2.10E+04	2.93E+03	7.12E+02	6.38E+01	2.57E-02	5.37E-07	4.80E-08
	3.33E-03	7.50E-04	1.63E+03	1.62E+04	1.84E+03	5.79E+01	4.71E+00	2.58E-02	5.38E-07	4.38E-08
	3.33E-03	1.00E-03	6.83E+02	1.69E+04	2.21E+03	1.82E+01	1.82E+01	2.57E-02	5.36E-07	4.64E-08
Oil	8.33E-05	2.00E-04	2.31E+03	2.62E+04	4.68E+03	1.04E+04	5.62E+02	2.10E-02	1.45E-08	7.85E-10
	8.33E-05	4.00E-04	3.00E+02	9.70E+03	1.02E+03	6.76E+02	4.76E+01	2.19E-02	1.51E-08	1.06E-09
	8.33E-05	7.50E-04	4.48E+01	7.98E+03	5.08E+02	5.38E+01	1.25E+00	2.15E-02	1.49E-08	3.44E-10
	8.33E-05	1.00E-03	1.90E+01	6.61E+03	5.83E+02	1.71E+01	5.86E-01	2.16E-02	1.49E-08	5.12E-10
	8.33E-04	2.00E-04	2.19E+04	9.03E+04	2.79E+04	9.86E+04	3.37E+03	2.22E-01	1.38E-07	4.71E-09
	8.33E-04	4.00E-04	2.70E+03	3.82E+04	4.83E+03	6.08E+03	4.00E+02	2.19E-01	1.36E-07	8.94E-09
	8.33E-04	7.50E-04	4.13E+02	2.53E+04	3.97E+03	4.95E+02	2.48E+01	2.21E-01	1.37E-07	6.85E-09
	8.33E-04	1.00E-03	1.74E+02	2.18E+04	3.65E+03	1.57E+02	7.29E+00	2.21E-01	6.36E-09	6.36E-09
	1.67E-03	2.00E-04	4.32E+04	2.38E+05	3.50E+04	1.94E+05	1.47E+04	4.37E-01	2.71E-07	1.58E-08
	1.67E-03	4.00E-04	5.43E+03	5.40E+04	3.44E+03	1.22E+04	6.83E+02	4.40E-01	2.73E-07	1.53E-08
	1.67E-03	7.50E-04	8.24E+02	6.52E+04	3.91E+03	9.88E+02	5.53E+01	4.40E-01	2.73E-07	1.53E-08
	1.67E-03	1.00E-03	3.46E+02	2.44E+04	3.34E+03	3.09E+02	3.63E+01	4.39E-01	1.72E-08	1.72E-08
	3.33E-03	2.00E-04	8.61E+04	4.50E+05	6.54E+04	3.86E+05	3.15E+04	8.70E-01	5.41E-07	4.39E-08
	3.33E-03	4.00E-04	1.08E+04	9.46E+04	1.11E+04	2.42E+04	1.76E+03	8.73E-01	5.41E-07	3.93E-08
	3.33E-03	7.50E-04	1.63E+03	4.71E+04	5.31E+03	1.96E+03	1.41E+02	8.73E-01	5.41E-07	3.91E-08
	3.33E-03	1.00E-03	6.88E+02	5.33E+04	7.55E+03	6.19E+02	6.19E+02	8.72E-01	5.40E-07	4.07E-08

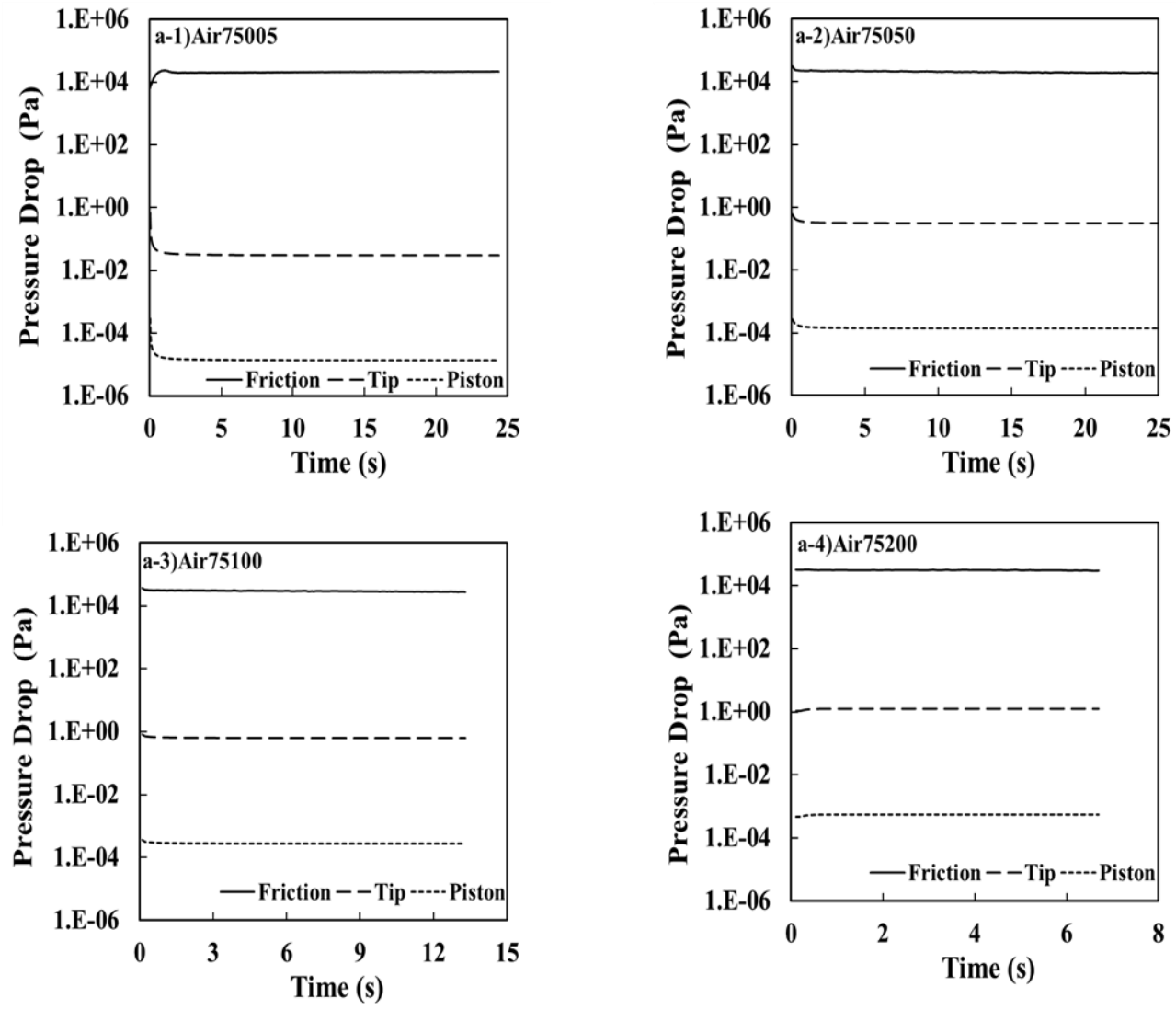

Figure 2.4: Pressure drop of friction, piston, and tip for air with a nozzle tip size of 7.5×10^{-4} m at velocities of presses at 8.3×10^{-5}, 8.3×10^{-4}, 1.7×10^{-3}, and 3.3×10^{-3} m/s.

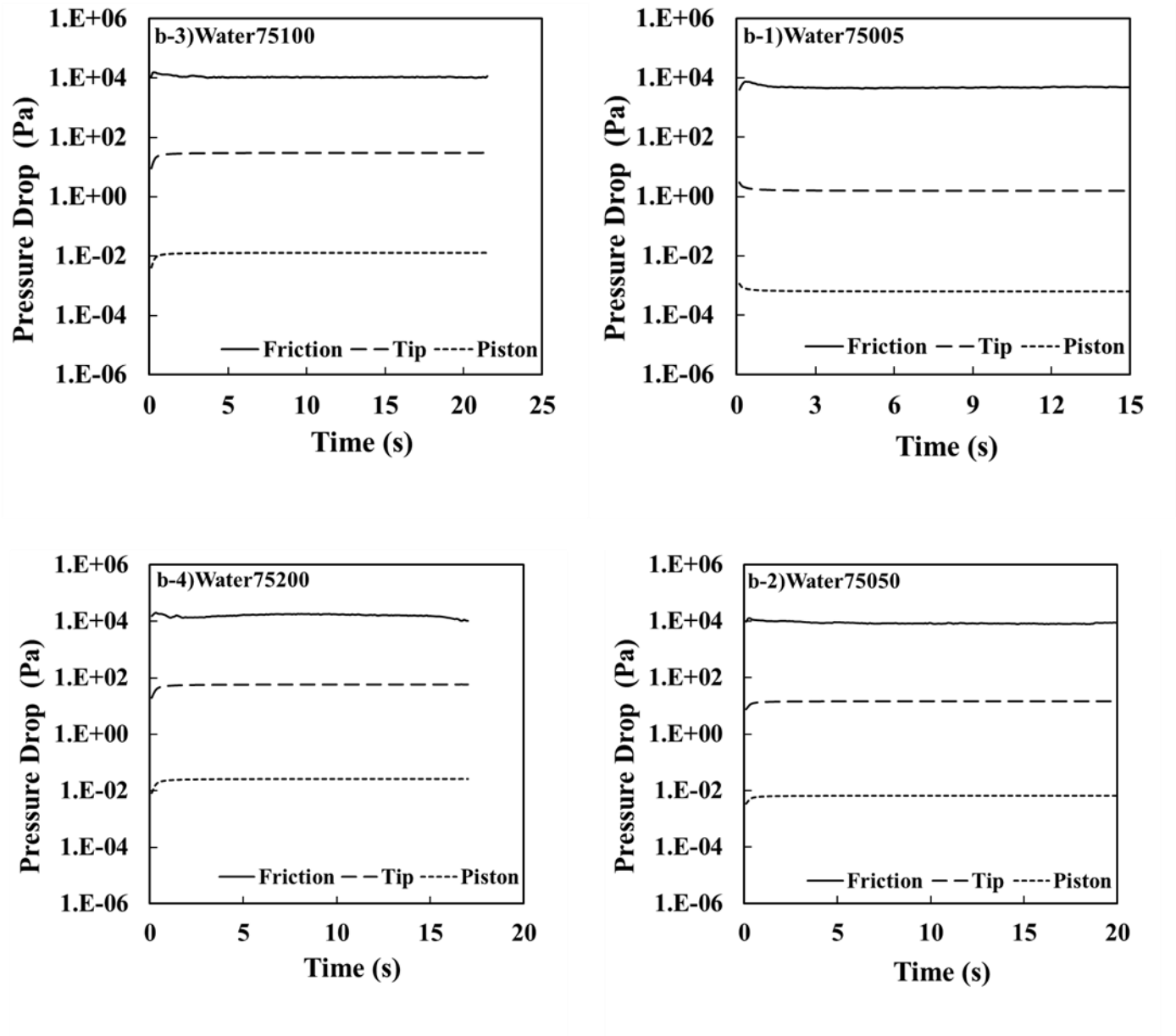

Figure 2.5: Pressure drop of friction, piston, and tip for water with a nozzle tip size of 7.5×10^{-4} m at velocities of presses at 8.3×10^{-5}, 8.3×10^{-4}, 1.7×10^{-3}, and 3.3×10^{-3} m/s.

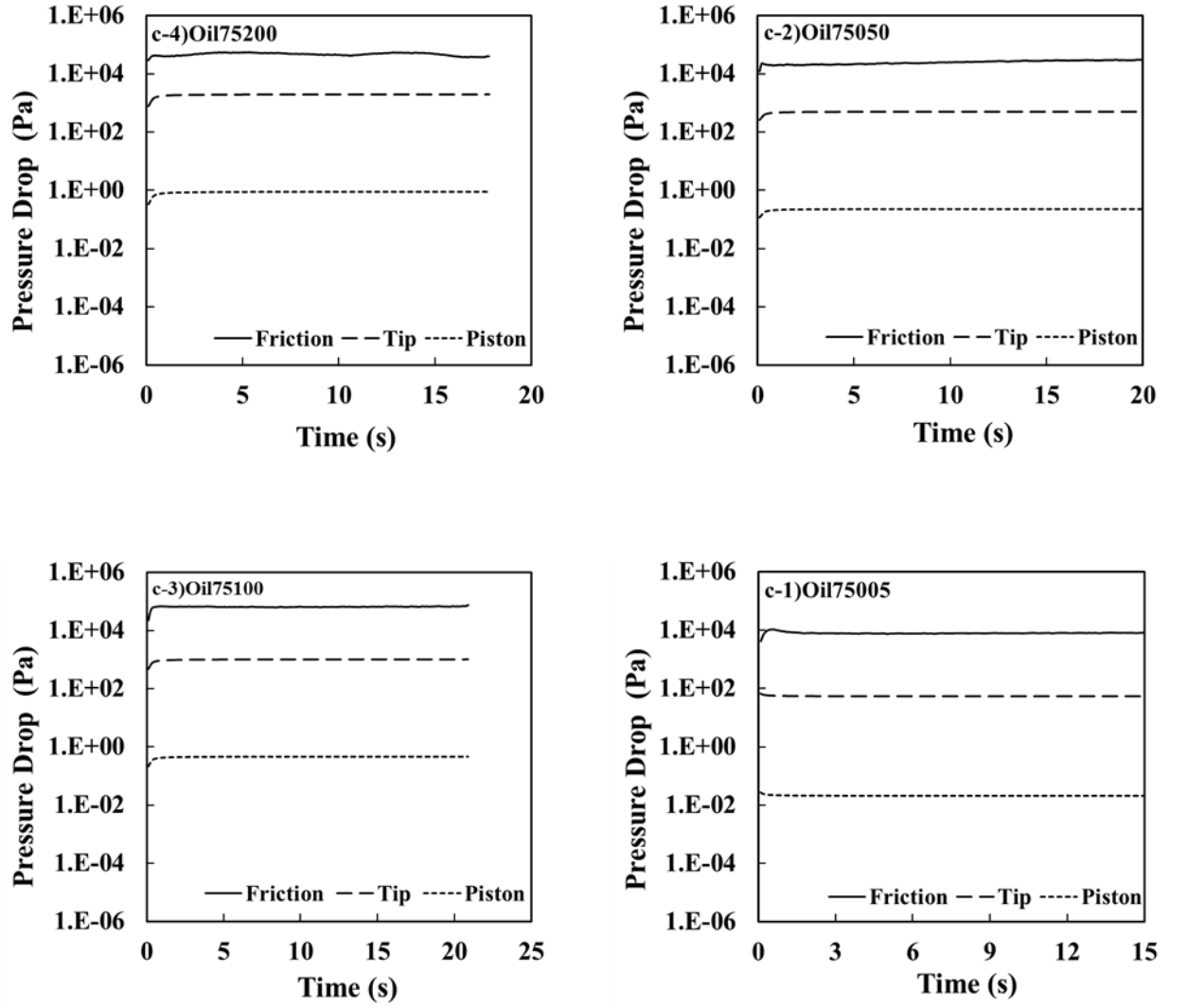

Figure 2.6: Pressure drop of friction, piston, and tip for oil with a nozzle tip size of 7.5×10^{-4} m at velocities of presses at 8.3×10^{-5}, 8.3×10^{-4}, 1.7×10^{-3}, and 3.3×10^{-3} m/s.

It is evident from preliminary results that the pressure drop due to friction ($\Delta P_{Friction}$) between the piston and the cylinder wall does not exhibit significant variation than the other two pressure drops. (Figure 2.4, 2.5, 2.6) Despite the change in material, nozzle tip size, and the velocity of the press, the $\Delta P_{Friction}$ experiences negligible fluctuation in the values. The above graphs were plotted for different press velocities of 8.3×10^{-5}, 8.3×10^{-4}, 1.7×10^{-3}, and 3.3×10^{-3} m/s. However, the tip size of radius 7.5×10^{-4} m remained for all. It is clear that $\Delta P_{Friction}$ remains almost

the same, but it is the highest value of the other two pressure drops. It is crucial to learn the pressure drop due to friction ($\Delta P_{Friction}$)in other words, the machines' own friction is the critical factor in material extrusion.

Along with pressure drop, the shear rate plays a crucial role in material extrusion. Understanding the change of $\Delta P_{Friction}$ with shear rate is necessary for the efficient quantitative discharge of the material. The $\Delta P_{Friction}$ changes are observed for shear rates ranging from 10 -10^5 s^{-1} for air, water, and hemp oil. (Figure 2.7) The $\Delta P_{Friction}$ of air, water, and hemp oil remains almost similar at a lower shear rate below 10^3 s^{-1}. However, for shear rates ranging from 10^3 -10^5 s^{-1}, the $4\Delta P_{Friction}$ grows ever so slightly for air and water, but more in the case of oil. Though the changes in $\Delta P_{Friction}$ are observed with shear rate, it is not significant for the printing process if a low shear rate is maintained. Further experimentation with materials having a higher viscosity than hemp oil was based on the assumption that if a constant force is applied equal to or higher than $\Delta P_{Friction}$ itself, ΔP_{Tip}, ΔP_{Piston} can be calculated by HP equation, and material can be extracted at a constant linear velocity provided the shear rate is lower than 10^3 s^{-1}.

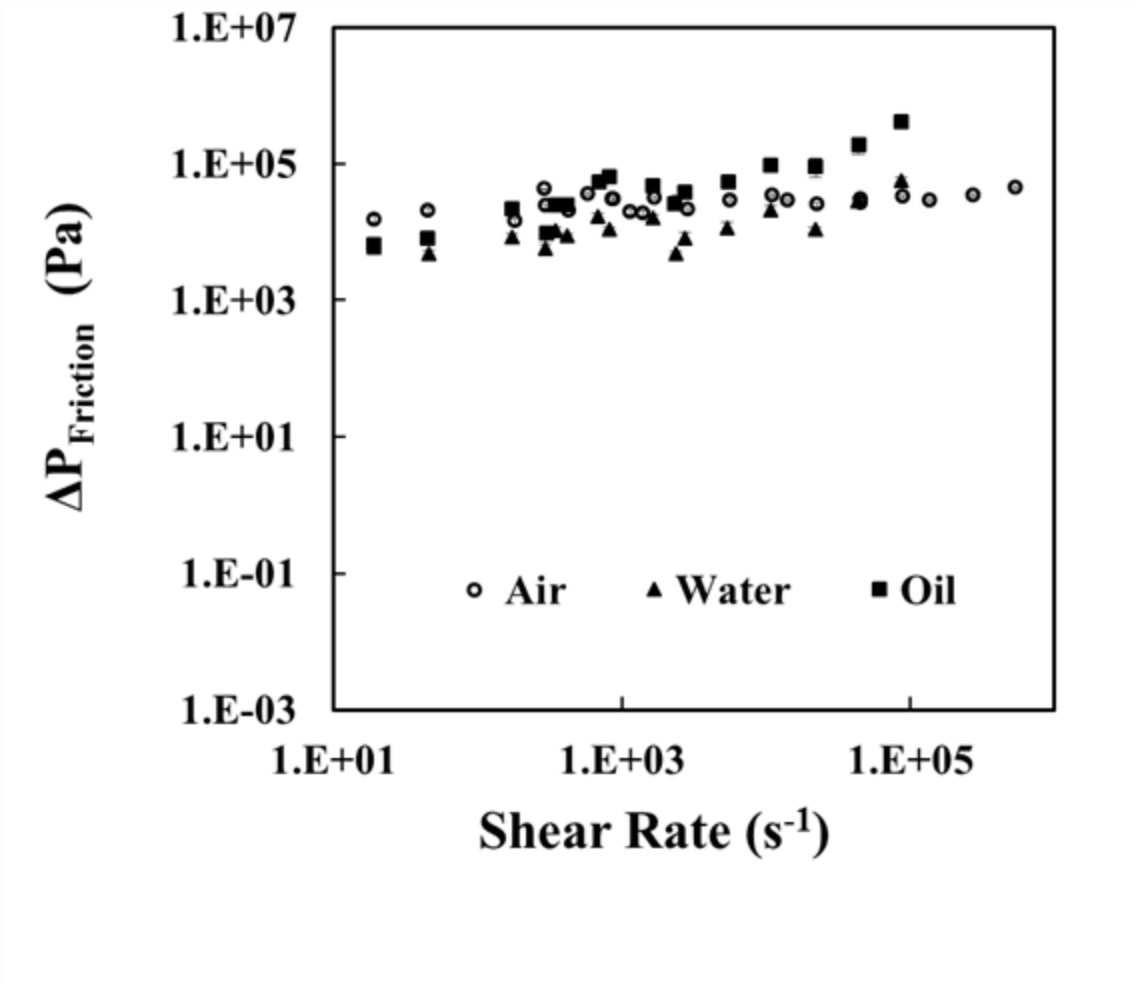

Figure 2.7: Pressure drop due to friction in terms of various shear rates of the piston-type extruder for Air, Water, and Oil.

The nozzle tip size is an additional factor that contributes to the pressure drop, then leading to the constant material deposition. Hydraulic and pneumatic methods with an external power source are always an option when materials with high viscosity have to be extruded through a smaller nozzle tip. For the current experimental setup, economic feasibility is one of the focal points, cannot accommodate such extrusion methods. The experiment was carried out with four nozzle tip sizes (r_{Tip}) of radius 2.0×10^{-4}, 4.0×10^{-4}, 7.5×10^{-4}, and 1.0×10^{-3} m. to check the press drop at the nozzle tip (ΔP_{Tip}). (Figure 2.8)

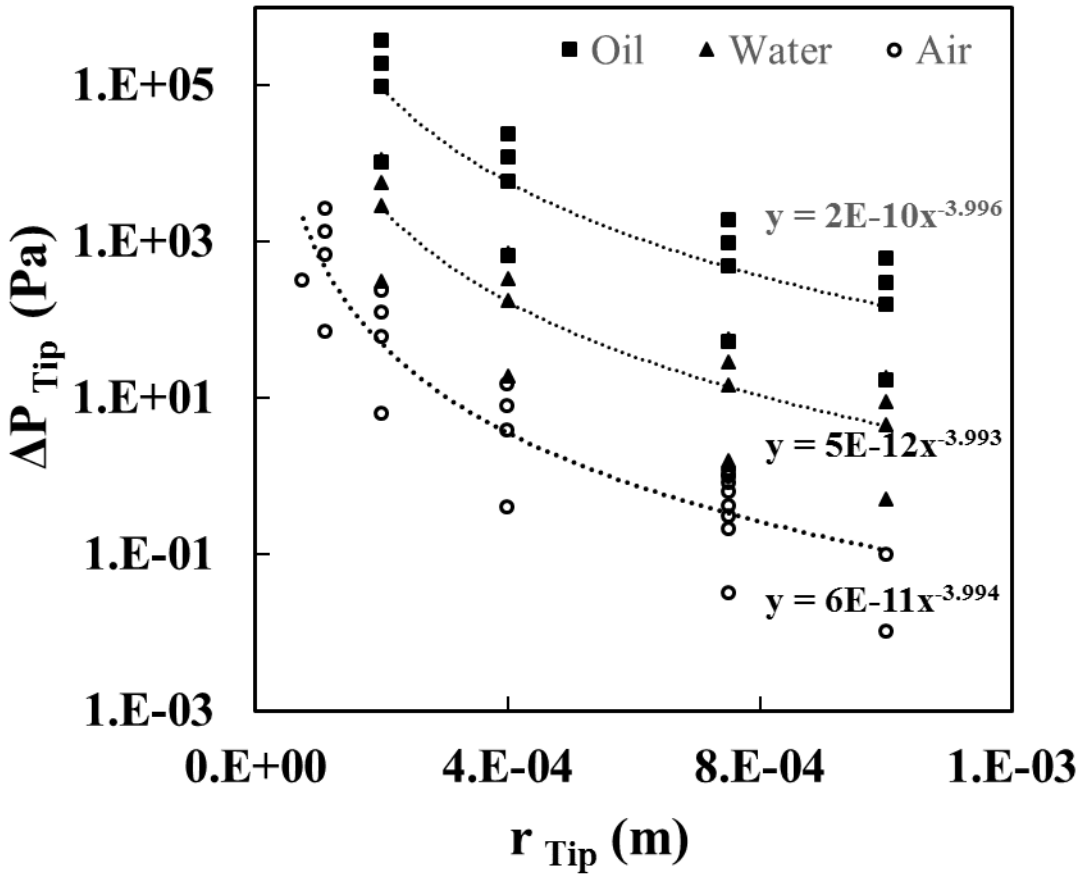

Figure 2.8: Pressure drop at nozzle tip for air, water, and hemp oil.

The expressions for pressure drop at the nozzle tip (ΔP_{Tip}), shear rate (γ), and linear velocity of the extruded material (v_z) are shown below.

$$\Delta P_{Tip} = \frac{8\mu(L_{Tip})q_w}{\pi\rho(r_{Tip})^4}$$

$$\gamma = \frac{4v_z}{r_{Tip}}$$

$$v_z = \frac{q_v}{\pi(r_{Tip})^2}$$

Combining and rearranging the equation, an expression for pressure drop in terms of nozzle tip size is obtained.

$$\Delta P_{Tip} = \frac{2\mu(L_{Tip})}{(r_{Tip})} \times \gamma$$

According to the HP equation, The ΔP_{Tip} is inversely proportional to the 4th power of r_{Tip}. Experimentally, the ΔP_{Tip} was reduced to 3.996, 3.993, 3.994 power of r_{Tip} for hemp oil, water, and air, respectively, for the nozzle tip sizes. It was experimentally confirmed that applying constant pressure and selecting an appropriate nozzle tip size could result in constant material discharge. Though the experiment was based on expressions for Newtonian materials, constant discharge of high viscous materials was successfully achieved.

The data obtained by repeated experiments as tabulated in Table 2.2 after calculating using HP equation is used to plot a logarithmic graph of ΔP_{Tip} and shear rate. (Figure 2.9)

$$\log(\Delta P_{Tip}) = \log\left[\frac{2\mu(L_{Tip})}{(r_{Tip})}\right] + \log(\gamma)$$

The y-axis and slope values are directly related to the dynamic viscosity of the material being extruded. The viscosity of the materials, air, water, and hemp oil used in this experiment is known, and the calculated values can be verified. This concept can be used to calculate the dynamic viscosities of fluids that have to be printed. The experiments with air, water, and hemp oil, the values of slopes 1.2180, 1.2181, and 1.2665 and values related to viscosity, -3.7579, -1.9556, and -0.4235, respectively, were obtained. On the calculation of the empirical data, the viscosities for air, water, and hemp oil were $(3.57\pm 0.170)\times10^{-2}$, $(1.06\pm 0.049)\times10^{-3}$, and $(1.97\pm 0.259)\times10^{-5}$ Pa.s.

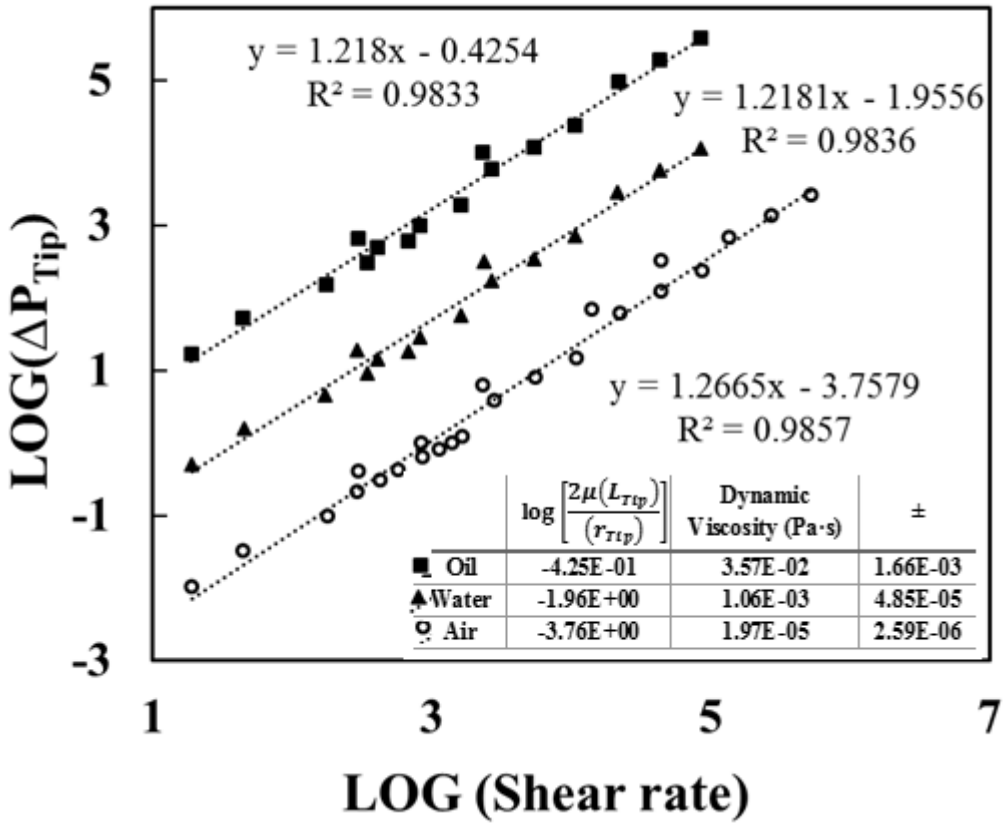

Figure 2.9: Log (ΔP_{Tip}) vs. Log (shear rates) for the piston-type extruder for Air, Water, and Oil.

Quantitative material discharge of fluids is complex as it depends on the nozzle tip size and the shear rate. The friction coefficient of a material is different from when it is still and in motion. Further, the viscosity, porosity, and friction coefficient changes with pressure and time. It is theoretically and experimentally challenging to account for changes due to its complex nature. Analysis through repeated experimentation with similar printing conditions with varying nozzle tip sizes and the velocity of the press was the way to proceed. Irrespective of the head travel speed (HTS), the material cannot be discharged faster than 0.1 m/s. The mismatch of the HTS with the material discharge speed results in an unfavorable print outcome. The HTS must co-relate with the material discharge to avoid discontinuous printing or excessive material deposition. As illustrated in Figure 2.10, if the material discharge rate is faster than the HTS, excess material is deposited in

the path resulting in a meandering thread-like appearance. On the other hand, if the HTS is greater than the material discharge speed, the material is scarcely deposited with discontinuities.

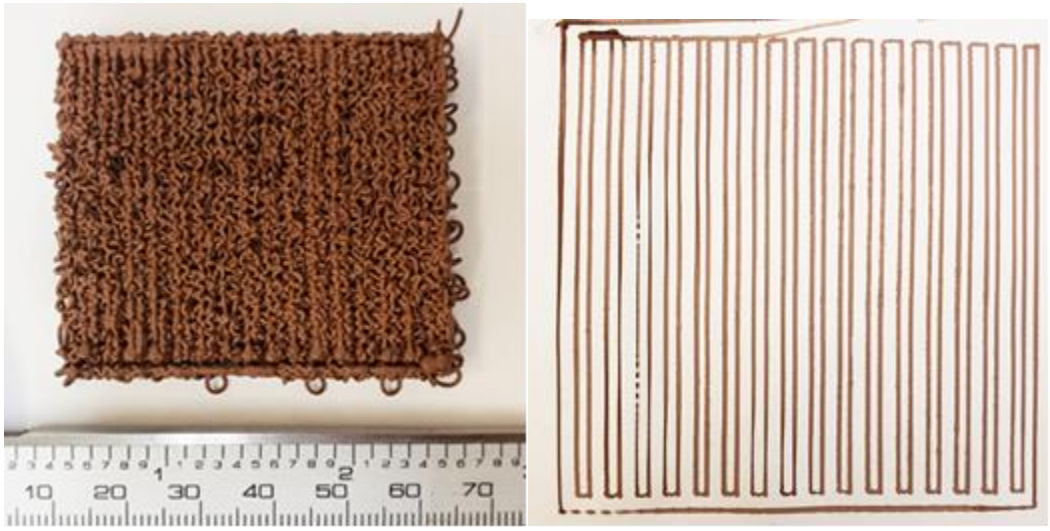

Figure 2.10: Images due to mismatch of head travel speed (HTS) versus material discharge speed, left- 2 (HTS): 1, right- 1 (HTS): 0.8.

The stepping motor used in this study has a maximum torque limit of 1.5 N.m. Extruding materials of higher viscosity through a small nozzle tip size is deemed as a limitation. The HP equation gives the means to calculate the pressure drop at the nozzle tip leading to shear rate. Iterative experiments suggested the relationship between the linear velocity and the shear rate is vital for printing high viscosity fluids with smaller force applied to the piston. For real-world applications of using such a small stepping motor to print high viscous fluids, the acquired data suggests for a given nozzle tip size and linear discharge velocity of 0.1 m/s; the shear rate must be less than 600 s^{-1}. (Figure 2.11)

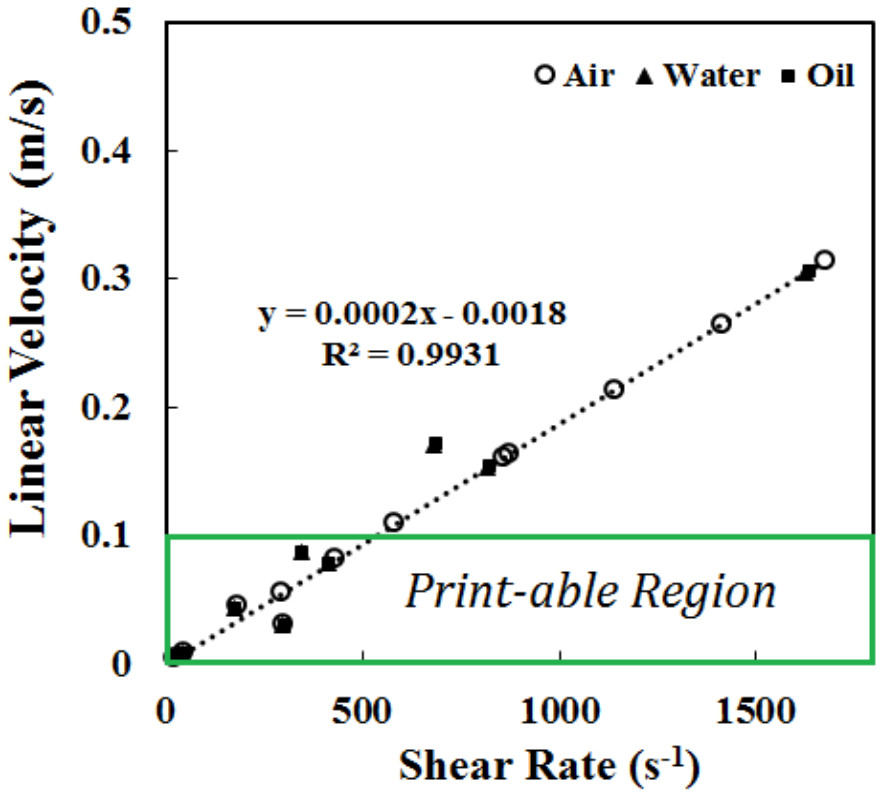

Figure 2.11: Print-able region in terms of linear velocity vs. various shear rates of the piston-type extruder for Air, Water, and Oil.

Chapter 3: 3D printing high viscosity materials.

3.1 Material preparation

Food printing is a topic in vogue, and massive research and demand for the technology are steadily rising. 3D printing of high viscosity materials fits perfectly with the ongoing research movement. There is a need for such technology in various fields, including biomedical, pharmacy, and telemedicine. Most AM machines that are commercially available deal with solid build material, and there are not many capable of printing fluids.

Many food ingredients are high viscous fluids and are readily available. Materials for this study include clay, ketchup, ranch, mayonnaise, chocolate, cookie dough, peanut butter, cheese, yogurt, ice cream, coffee, vegetable oil, hemp oil, (cannabidiol) CBD oil, fruit jam, all-purpose flour, and meat, including beef and chicken, which were procured commercially. Most of the food ingredients do not require pre-experimental preparation. However, meat products require preparation to make them flow through the nozzle.

In December 2020, the United Nations (UN) voted to remove cannabis from a category of the world's most dangerous drugs for medicinal purposes.[1] Few products of cannabis display vicious fluidity and are potential materials that can be used in this research. Hemp oil and CBD oil are the derivatives of cannabis and are used for research purposes only.

3.1.1 Supercritical fluid (SCF) extraction of meat

Supercritical fluid (SCF) extraction of meat quickly and safely removes the residual blood from the meat leaving behind healthy meat. Carbon dioxide is used as a solvent for SCF extraction. For the SCF extraction process, 5.00±0.50g of chicken and beef is pulverized at 6,000~24,000 RPM over five minutes cycles using NINJA® meat-grinder. Multiple pulverization cycles are

[1] https://news.un.org/en/story/2020/12/1079132

necessary to achieve the required consistency for the process. According to the experiment, three pulverization cycles were sufficient to ensure the chunk size is no larger than 5.0×10^{-5} m. To prevent degradation of the meat, it is refrigerated at -20℃ in plastic bags until use.

As seen in Figure 3.1, the sample is placed in an extraction vessel, and CO_2 along with cosolvents are passed through it. The solvents dissolve the residual blood and cholesterol from the meat and accumulate in the collecting vessel on the lower end of the tilted extraction vessel. The extraction time is about 40 minutes with pressures at (2.03×10^7Pa, 3.04×10^7Pa, and 4.05×10^7Pa) and at temperatures 35±5℃ or 50±5℃. The left-behind meat sample is devoid of residual blood, and cholesterol is a healthy option for consuming meat. (Figure 3.2)

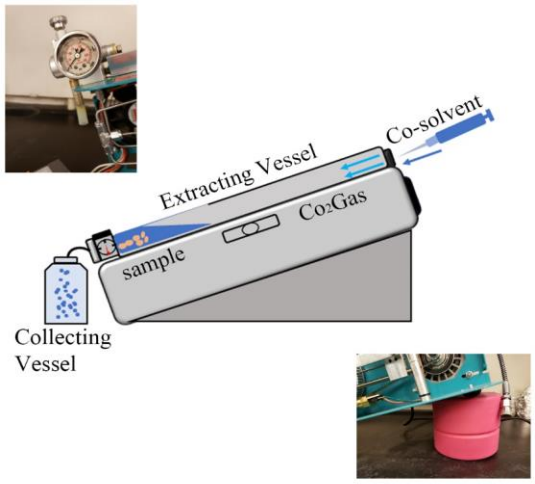

Figure 3.1: Conceptual drawing of the supercritical extraction system and image of the OCO-LABS part, including collection vessel, sample extraction vessel, and pressure monitor.

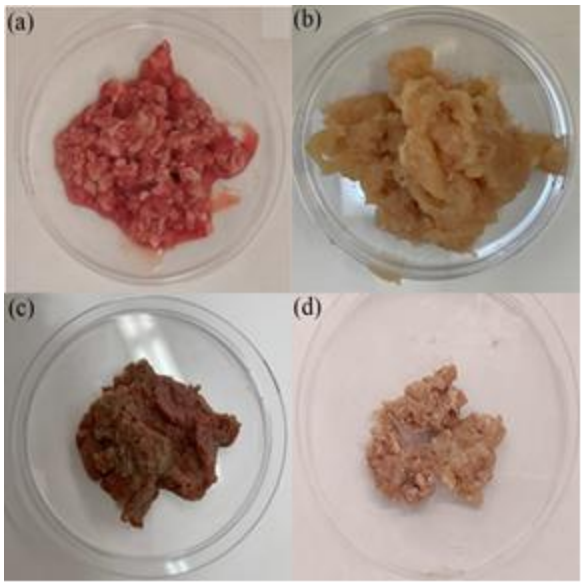

Figure 3.2: The samples; (a): unprocessed beef; (b): unprocessed halal chicken; (c): unprocessed halal beef; (d): SC-CO2 processed beef under pressure at 3.04×107Pa and temperature at 50±5℃.

Further blood diffusion in water analysis was conducted for visual verification of blood extraction from the meat. The SCF extracted samples are compared with other untreated meat to check for the difference in the color. (Figure 3.3) The darker shade of red color in the water suggests more blood remnants in meat, and the lighter shade of red color signifies lower blood content.

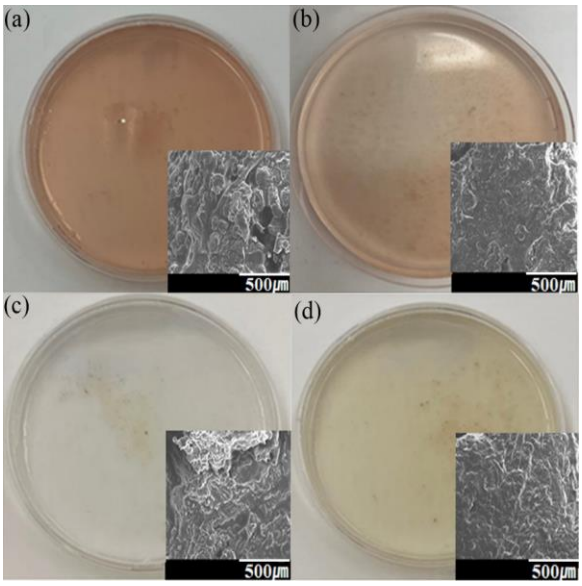

Figure 3.3: Images of blood diffused in water, SEM (a): unprocessed beef (b): unprocessed halal beef (c): SCF under pressure at 3.04×10^7 Pa processed with water as a cosolvent (d): SCF under pressure at 3.04×10^7Pa processed with oil as a cosolvent

In the SCF process's meat treatment, the high temperature and extraction pressure increase the process efficiency by 22.5%, but the use of a cosolvent has confirmed the effect of reducing the meat weight by up to 39.4%. The reduction of weight signifies the removal of blood and cholesterol, leaving behind the essential meat for dietary consumption. Apart from removing residual blood and cholesterol from the meat, the SCF processed meat has a consistency similar to porridge. This consistency is favorable for the 3D printing of meat as it can hold the three-dimensional structure.

3.2 DESIGN AND ACCESSIBILITY

3.2.1 Computer-aided designing (CAD)

Digital designs are the starting point of any 3D printing process. The digital designs for this study involved CAD software such as Solidworks, Solidedge, and Rhino 3D. The designs were created digitally using CAD software and saved as an STL file before using an open-source slicing

application called CURA. CURA slices the digital design into multiple layers and creates a G-code map for the 3D printer to navigate the extruder for the 3D printing operation. The 3D printer used in this study accepts the G-code and completes the 3D printing job promptly.

3.2.2 Single-line design (SLD)

3D printing of high viscous fluids is complicated due to the inherent nature of their flow properties. The typical stop and start operation performed by the filament feeder mechanism cannot be applied to print high viscous fluids. A unique printing mechanism was necessary to accommodate the lethargic flow of high viscous fluids. Single line design (SLD) was the solution to curb the issue of undesirable flow. SLD traces a path that is not passed over again while creating the image in the process. (Figure 3.4) SLD considerably reduces the amount of material overlapping and resolves uneven material deposition caused by stop-and-go.

Figure 3.4: Single line designs (SLD) of sceneries.

SLD offers faster 3D printing speed to lower the oxidation or degradation of few high viscous fluids susceptible to exposure to the atmosphere for a prolonged time. The application of this concept helps the 3D printing process and preserves the artistic values of the design.

3.2.3 Integration of the internet of things (IoT)

The Raspberry Pi installed in the 3D printer is an onboard computer that can access the web to acquire design data for printing. The ability of the 3D printer to access the web brings it under the canopy of IoT. The integration of IoT in the 3D printers enhances accessibility and simplifies the 3D printing process. The 3D printers integrated with IoT allow long-distance printing where the print order can be given without physically being present at the site. This feature opens the door for numerous possibilities and unbound applications across all walks of life.

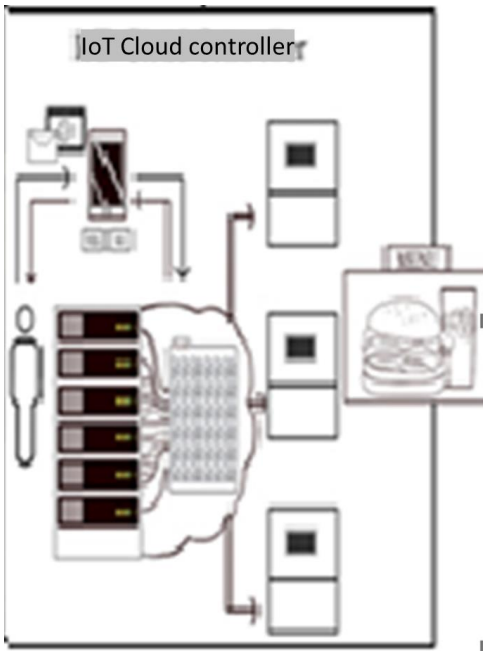

Figure 3.5: Schematic diagram of IoT integrated 3D printing concept

The concept of an IoT-enabled 3D printer network is as shown in Figure 3.5. The website can be accessed through any device with an internet connection. (Figure 3.6 Left) Online portals can be accessed at http://www.cafeboxd.com; http://www.vizovizo.com/; and http://www.bm3dp.com/. Once signed in, access to numerous creative designs is provided. A new design or one of the numerous existing creative designs from the catalog can be browsed and

selected for printing remotely. (Figure 3.6 Right) When the design is selected, an order is sent under the account name and saved in the cloud. The interface allows sharing text, images, videos, or combining those under the same account.

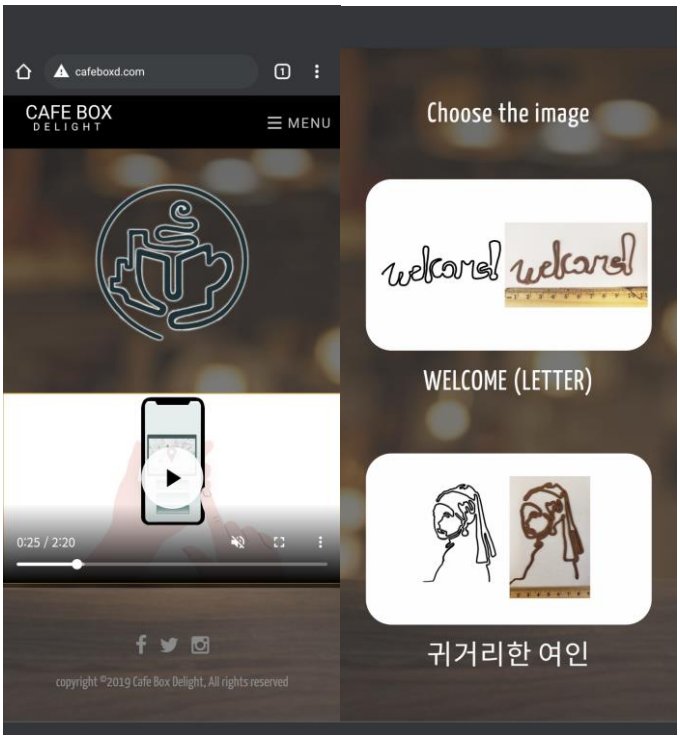

Figure 3.6: Left: Online portal for ordering the 3D printable design remotely. Right: Online catalog of designs.

An order can be placed for self-pick-up or someone else. It is not necessary to be physically present to place the order as it is accessible through the internet but has to be on-site to collect the printed product. The ordered design is saved on the cloud until it is opened at one of the IoT integrated 3D printers for printing. (Figure 3.7 left) The screen on the 3D printer can display the media shared by the person placing the order. (Figure 3.7 Right) There are in total of 17 IoT-controlled 3D printing systems. Four systems at the K-CBD Center in Seoul, Korea Four systems at Café Box Delight in Seoul, Korea; three units in Anam International house, Seoul, Korea; two

systems at Maker's Station in TX, USA; Four systems at the University of Texas at El Paso, Texas, USA.

Figure 3.7: Left: Accessing the remote printing. Right: Playing shared media on-screen while printing.

3.3 3D PRINTING

The data obtained by applying the HP equation from the iterative experiments provided insight into the amount of compression needed for the piston and HTP for a constant material extrusion necessary for a smooth continuous flow. By adjusting the values of the z-axis, 2D and 3D printing can be performed with a single material stand-alone print and also print on an object's surface. Muti-layer-multi-material stacking operation can also be performed by interchanging the cartridge between the material switch. The precise control over the printing process allows the 3D printer to print scaled-down models of objects. This technique is helpful in the food industry to fill the condiments on the food artistically. The nozzle tip size may vary depending on the viscous fluids that are being printed. HTS and the material discharge velocity according to the pressure applied on the piston are crucial to maintaining the operating conditions and for smooth material

flow. The printing time drastically reduces with an increase in HTS, as shown in Figure 3.8, but it does not have a negative effect on the final print.

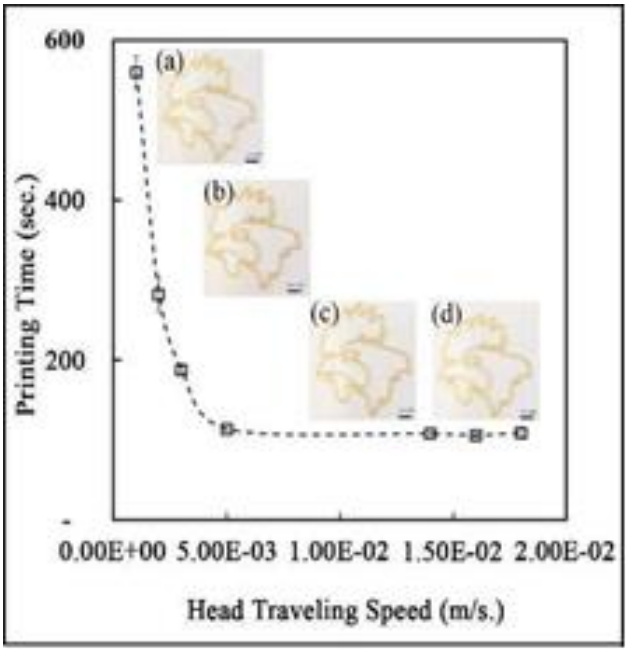

Figure 3.8: (a) HTS: 1.0×10^{-3}m/s (b): HTS: 5.0×10^{-3}m/s, (c): HTS: 1.5×10^{-2} m/s and (d): HTS: 1.8×10^{-2} m/s

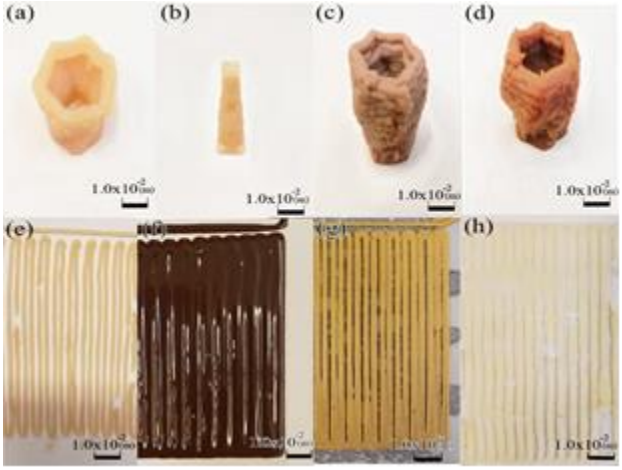

Figure 3.9: (a): 3D printed vase design with Halal chicken. (HTS: $1.8x10^{-2}$m/s and tip size $1.0x10^{-3}$m), (b): 3D printed Chun-Sung-Dae design with Halal chicken. (HTS: $7.0x10^{-3}$m/s and tip size $3.2x10^{-4}$m), (c): 3D printed vase design with SCF treated beef sample. (HTS: $1.8x10^{-2}$m/s and tip size $1.0x10^{-3}$m) (d): 3D printed vase design with Halal beef. (HTS: 1. $8x10^{-2}$m/s and tip size $7.5x10^{-4}$m), (e): 2.5 D printed grid line with SCF Processed beef. (HTS: $1.8x10^{-2}$m/s and tip size $1.0x10^{-3}$m), (f): 2.5 D printed grid line with chocolate. (HTS: $1.8x10^{-2}$m/s and tip size $1.0x10^{-3}$m), (g): 2.5 D printed grid line with peanut butter. (HTS: $1.8x10^{-2}$m/s and tip size $1.0x10^{-3}$m) and (h): 2.5 D printed grid line with potato. (HTS: $1.8x10^{-2}$m/s and tip size $1.0x10^{-3}$m).

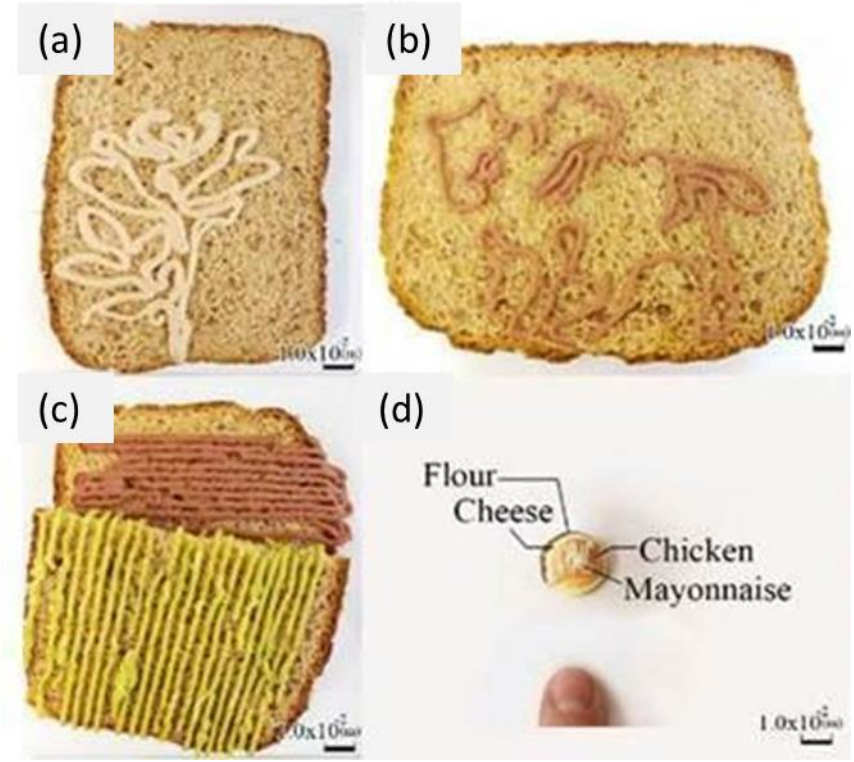

Figure 3.10: (a): CBD infused chicken, (HTS 1.8×10-2m/s and tip size 1.0×10-3m); (b): CBD infused SCF extracted beef, (HTS 1.8×10-2m/s and tip size 1.0×10-3m); (c): CBD infused Avocado Sandwich with SCF extracted beef (HTS 1.8×10-2m/s and tip size 1.0×10-3m), and CBD infused Avocado. (HTS 1.8×10-2m/s and tip size 1.0×10-3m); (d): CBD infused chicken burger; flour dough (HTS 1.8×10-2m/s and tip size 1.0×10-3m), cheese (HTS 7.0×10-3m/s and tip size 3.2×10-4m),. chicken (HTS 7.0×10-3m/s and tip size 3.2×10-4m) and mayonnaise. (HTS 7.0×10-3m/s and tip size 1.1×10-4m).

The HTS and the nozzle tip size vary according to the viscous material that is being printed. (Figure 3.9) A small amount of CBD was infused to show the potential of the 3D printer in the food industry. CBD is a dietary supplement and can now be 3D printed as CBD-infused 3D printed food. In Figure 3.10, CBD-infused food ingredients are 3D printed, and the HTS and the nozzle tip size are varied accordingly. A miniature chicken burger with a different material is stacked layer upon layer, displaying the precise control over the material discharge of the 3D printer.

Figure 3.11: Single line design printed with chocolate, coffee, ranch, mayonnaise, and ice cream at Center of Printable Materials (CPMC), UTEP, Texas, USA.

The artistic SLD was printed depicting an image or a word or a word through an image. (Figure 3.11) The material was deposited on paper or food placed on the printing platform. In Figure 3.11 (l), coffee is printed on froth in the shape of a penguin displaying the precise control of the head movement and the material flow through the nozzle. The integration of IoT makes it easy to transfer the digital design to a 3D printer located remotely. The 3D printer can access the design through the cloud and initiate the 3D printing process once the print request is accepted. SLDs and 3D structures can be remotely printed as shown in Figure 3.12; also, 3D printing was successfully carried out across two continents between UTEP, Texas, USA, and Korea University, Seoul, South Korea. (Figure 3.13)

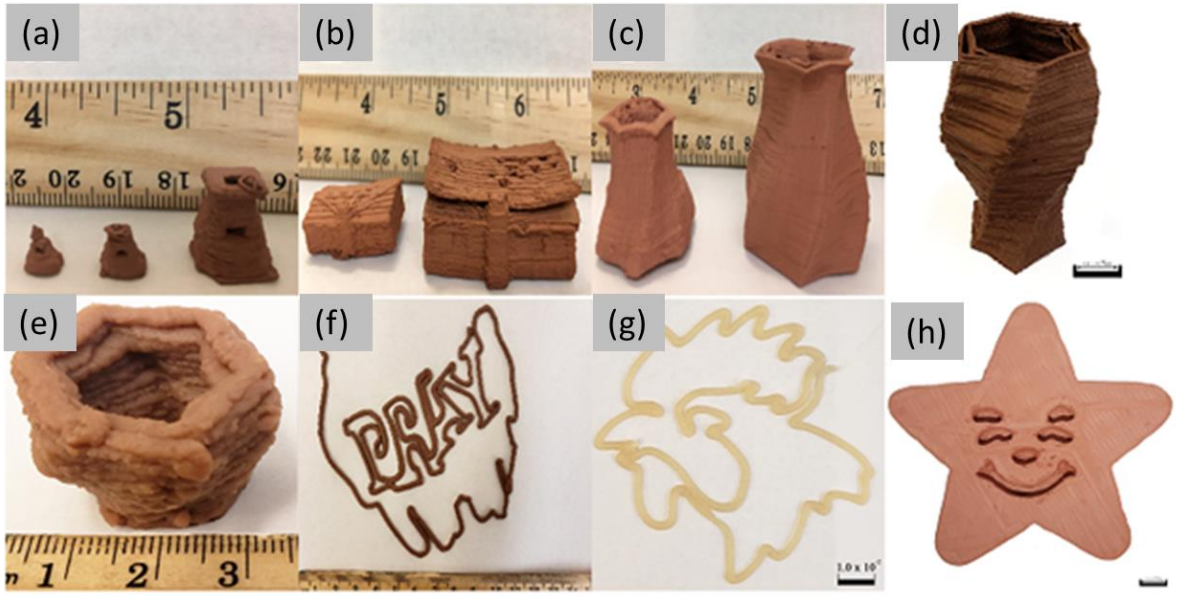

Figure 3.12:(a),(b),(c) Miniature 3D objects printed with clay; (d) Miniature 3D flower vase printed with chocolate; (e) Miniature 3D flower vase printed with beef; (f), (g) SLD with chocolate and mayonnaise; (h) 3D printed design with chocolate.

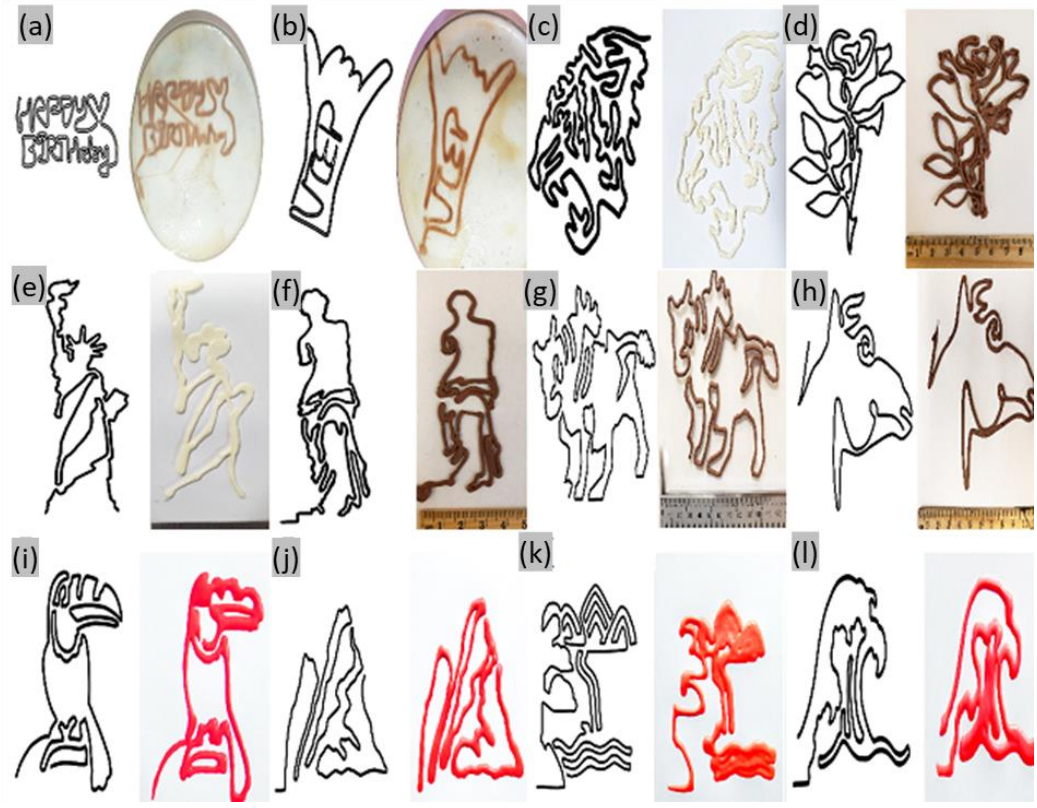

Figure 3.13: Digital SLD sent from UTEP, Texas, UAS to Korea University, Seoul, South Korea, printed with coffee, chocolate, peanut butter, ranch, mayonnaise, and fruit jam.

Chapter 4: 3D printing on prosthetic teeth

4.1: Material preparation

The 3D printer with a piston-type extruder carries out the preparation of hydroxyapatite scaffolds, and the printability of the hydroxyapatite (HA) being the build material holds a crucial role. It is necessary for HA being a powder, to be in fluid form to flow through the nozzle when pressure is applied and also viscous enough to hold the shape after being printed. An observation indicated the slurry of HA with distilled water to be fluid and sticky. The moisture content in the build material poses an essential parameter for fluidity and printability. Few iterations suggested an optimum moisture percentage for a successful HA print.

The HA powder used in this study seems larger than the mentioned 20µm when observed under Scanning Electronic Microscope (SEM), as shown in Figure 4.1 A and B. The HA particles form clusters resulting in the appearance of bigger particle sizes. The declustering of HA particles through grinding caused the clusters to break down, but the process emerged excessively, forming a pancake shape, as shown in Figure 4.1 C&D.

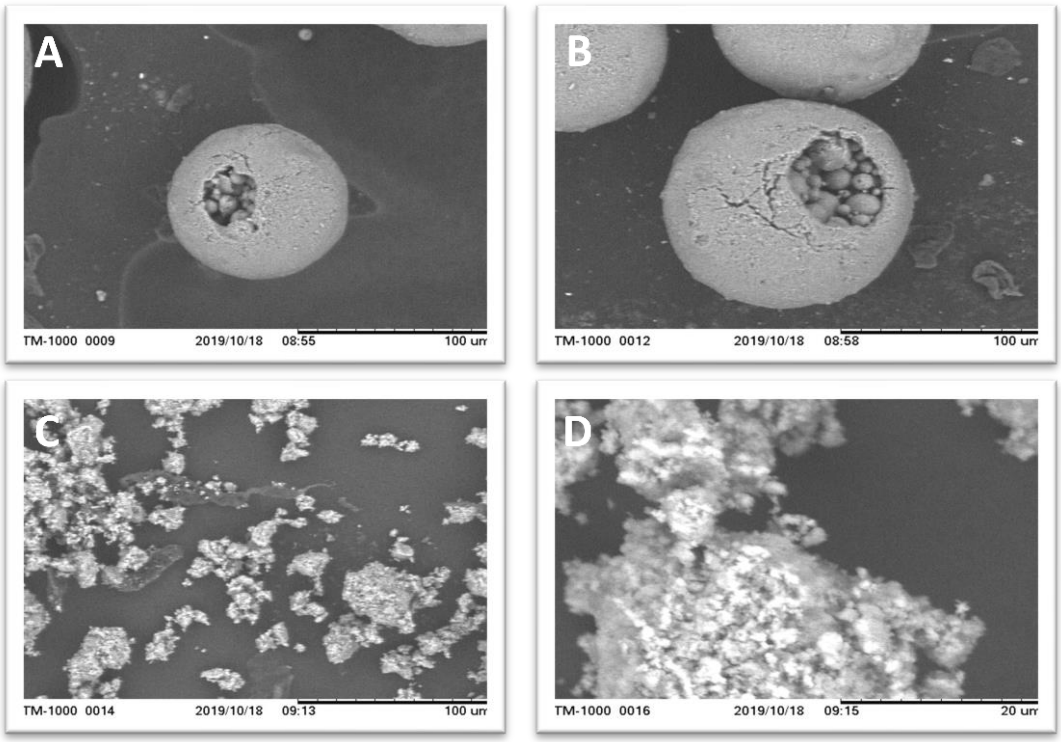

Figure 4.1: A&B: Hydroxyapatite powder samples in a cluster from; C&D: Hydroxyapatite powder after grinding.

The measurement of moisture being crucial for the printability, a specific quantity of HA powder mixed with distilled water subjected to heating for 15 minutes, weighed before and after heating to obtain moisture percentage. A couple of iterations of such a procedure suggested the required moisture percentage of the HA build material, which is 26%. Further, this mixture of water with HA powder was set aside for 24 hours to attain printable consistency.

4.2 PRELIMINARY SINTERING PROCESS

The green products from the 3D printer must undergo sintering at an appropriate temperature. This process is necessary for the resultant sample to attain practical mechanical properties to function as teeth. Exposure of HA to elevated temperatures of approximately 1250°C results in a dense structure. Hence, sintering at a comparatively lower temperature is required to

ensure porosity in the structure. Sintering temperature affects the porosity, which further reflects on the mechanical performance of the part. As a result, 3D printing of dog-bone HA structures followed by studying the effect of different sintering temperatures on the structure was necessary. Sintering temperatures of 600°C, 800°C, 1000°C, and 1050°C performed on HA dog-bone structure is as shown in Figure 4.2.

The result of varying sintering temperature on HA dog-bone structures showed black coloration at 600°C and 800°C, whereas at 1000°C and 1050°C, no such coloration exists. The presence of organic substances at lower sintering temperatures is responsible for the dark coloration of the samples. At higher temperatures, during calcination, the combustion of the organic substances, samples obtained appear white.

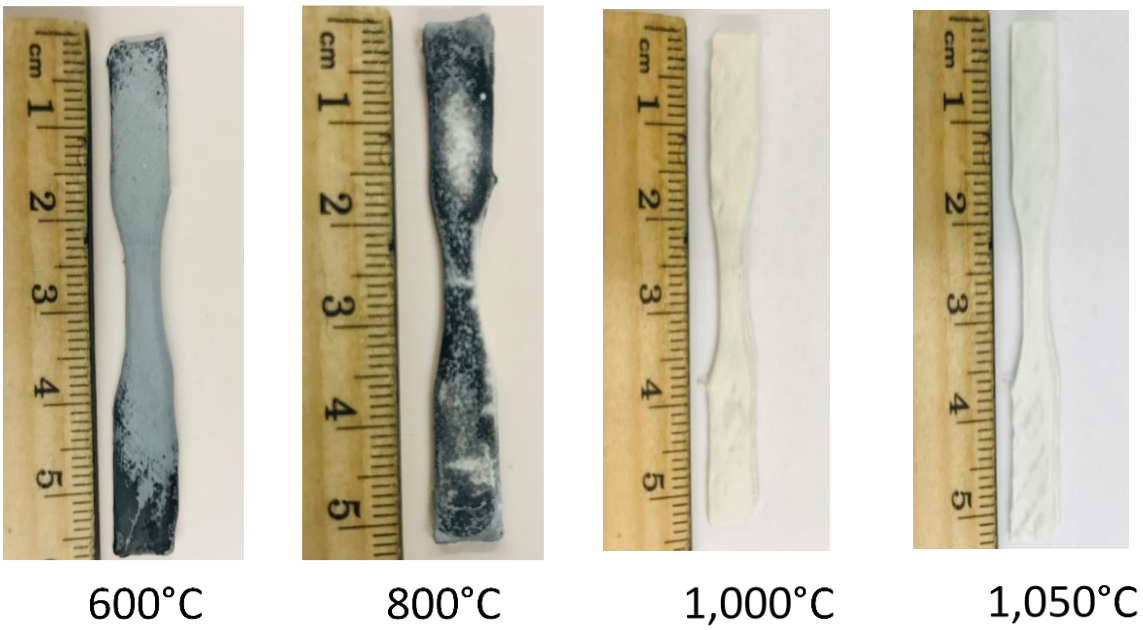

Figure 4.2: Dog-bone structures post sintering (600℃, 800℃, 1,000℃, 1,050 ℃) for 50mins.

4.3 3D PRINTING OF PROSTHETIC TEETH WITH HYDROXYAPATITE

The build material, after preparation, to attain the desirable moisture percentage with required printable consistency is filled up in the cylindrical tube with the piston on the other end. The 3D printer utilizes a piston-type extruder (PTE) to print. The current study is focused on the printing of HA scaffolds to conduct a cell study. The CAD design is an input for CURA slicing software and acquires the G code for the print. The G code enables the printer nozzle to navigate for the printing process. Once the printing is complete, the finished product, also called the green part taken out carefully and dried in atmospheric conditions for 24 hours to solidify completely. Post-processing such as sintering ensures the enhancement of the mechanical property of the green part. The demonstration of the ability of the 3D printer with PTE to print prosthetic teeth structure is evident in Figure 4.3.

Figure 4.3: Green part of human molar teeth (26% moisture content) printed at CPMC, UTEP.

The integration of IoT in 3D printing enables long-range/remote printing of teeth. The design was uploaded from UTEP, USA, to the cloud and stored at http://www.bm3dp.com/ for future access. The design was 3D printed after accessing from the cloud through the 3D printer located at the K-CBD center, Korea University, South Korea. After numerous experiments, for

HA slurry, the HTS was set at 1. $8x10^{-2}$m/s, and the nozzle tip size of $7.5x10^{-4}$m yielded the best results with print time of 162 s. (Figure 4.4)

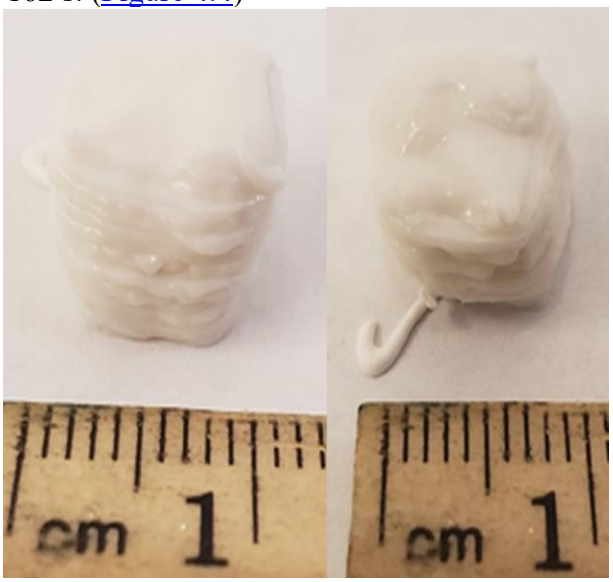

Figure 4.4: Green part of human molar teeth (26% moisture content) printed at K-CBD center, Seoul, South Korea. (HTS: 1. $8x10^{-2}$ m/s, and the nozzle tip size of $7.5x10^{-4}$m)

Chapter 5: Conclusions

The trajectory of the ongoing research on 3D printing technologies is leading towards the innovation of machines that can overcome material limitations. This research set out to explore the possibilities of making 3D printers efficiently and economically print high viscosity materials. Material preparation is an essential step in the additive manufacturing (AM) process; meat preparation using the Supercritical fluid (SCF) extraction resulted in healthier meat and consistency favorable for 3D printing. Piston-type extruder (PTE), being the efficient and economical choice for 3D printing viscous fluids, was exploited. Iterative experimentations were conducted to gather data on Newtonian fluids such as air and water along with hemp oil, a non-Newtonian fluid. The Hagen- Poiseuille (HP) equation was applied to the collected data to analyze the behavior of the fluids. The analysis offered the relationship among pressure drop at different locations(ΔP_{Piston}, ΔP_{Tip}, and $\Delta P_{Friction}$), shear rate (γ), and nozzle tip size (r_{Tip}), which has a crucial role in continuous material flow from the extruder. The artistic approach of single-line design (SLD) reduced the unevenness in the print as it does not trace its path. The absence of a stop-and-go mechanism, the SLD improved the print time. The precise control over the heat travel speed (HTS) and the material discharge led to successful printing of several 2.5D and 3D prints along with miniature 3D objects. The proficiency in precision printing of viscous materials demonstrated the potential of the 3D printers in the medical, pharmacy, and food industries. The integration of the internet of things (IoT) with the 3D printers enabled remote and long-distance printing. Numerous designs were 3D printed across two continents, and the use of cannabidiol exhibited the potential of 3D printers in the food and telemedicine industries. The ability of the 3D printer to print human prosthetic teeth with hydroxyapatite (HA) witnessed, and dental scaffolds for cell study were remotely 3D printed.

References

1. Wong; K V., Aldo Hernandez. A Review of Additive Manufacturing.: EBSCOhost. http://web.a.ebscohost.com/ehost/pdfviewer/pdfviewer?vid=19&sid=a07f2ed9-410f-4c53-b297-b884d403a586@sessionmgr4005&hid=4101
2. 3D Printing Market Size to Reach Revenues of $29 Billion by 2025 | Arizton. https://www.arizton.com/market-reports/3d-printing-market
3. 52900:2015 A. Standard Terminology for Additive Manufacturing – General Principles – Terminology. *ASTM Int*. 2015;i:1-9. http://compass.astm.org/EDIT/html_annot.cgi?ISOASTM52900+15
4. Buchanan C, Gardner L. Metal 3D printing in construction: A review of methods, research, applications, opportunities and challenges. *Eng Struct*. 2019;180(October 2018):332-348. doi:10.1016/j.engstruct.2018.11.045
5. Chen Z, Li Z, Li J, et al. 3D printing of ceramics: A review. *J Eur Ceram Soc*. 2019;39(4):661-687. doi:10.1016/j.jeurceramsoc.2018.11.013
6. Wang X, Jiang M, Zhou Z, Gou J, Hui D. 3D printing of polymer matrix composites: A review and prospective. *Compos Part B Eng*. 2017;110:442-458. doi:10.1016/j.compositesb.2016.11.034
7. Comb JW, Priedeman WR, Turley PW. FDM Technology Process Improvements. *Proc Solid Free Fabr Symp*. Published online 1994:42-49.
8. Turner BN, Gold SA. A review of melt extrusion additive manufacturing processes: II. Materials, dimensional accuracy, and surface roughness. *Rapid Prototyp J*. 2015;21(3):250-261. doi:10.1108/RPJ-02-2013-0017
9. Crump SS. Apparatus and method for creating three-Dimensional objects. 1992;28(3).

doi:https://patents.google.com/patent/US5121329A/en

10. Rocha CR, Angel R. Torrado Perez, Roberson DA. Novel ABS-based binary and ternary polymer blends for materialextrusion 3D printing.pdf.

11. Mohamed OA, Masood SH, Bhowmik JL. Optimization of fused deposition modeling process parameters: a review of current research and future prospects. *Adv Manuf*. 2015;3(1):42-53. doi:10.1007/s40436-014-0097-7

12. Alafaghani A, Qattawi A. Investigating the effect of fused deposition modeling processing parameters using Taguchi design of experiment method. *J Manuf Process*. 2018;36(December 2017):164-174. doi:10.1016/j.jmapro.2018.09.025

13. Mahmood S, Qureshi AJ, Talamona D. Taguchi based process optimization for dimension and tolerance control for fused deposition modelling. *Addit Manuf*. 2018;21(March):183-190. doi:10.1016/j.addma.2018.03.009

14. Pavan Kumar G, Regalla SP. Optimization of support material and build time in fused deposition modeling (FDM). *Appl Mech Mater*. 2012;110-116(October):2245-2251. doi:10.4028/www.scientific.net/AMM.110-116.2245

15. Rayegani F, Onwubolu GC. Fused deposition modelling (fdm) process parameter prediction and optimization using group method for data handling (gmdh) and differential evolution (de). *Int J Adv Manuf Technol*. 2014;73(1-4):509-519. doi:10.1007/s00170-014-5835-2

16. Boschetto A, Bottini L. Roughness prediction in coupled operations of fused deposition modeling and barrel finishing. *J Mater Process Technol*. 2015;219:181-192. doi:10.1016/j.jmatprotec.2014.12.021

17. Huang J, Chen Q, Jiang H, et al. A survey of design methods for material extrusion

polymer 3D printing. *Virtual Phys Prototyp*. 2020;15(2):148-162. doi:10.1080/17452759.2019.1708027

18. H.A. Barnes, J.E Hutton, K. Walters F. R. S. *An Introduction to Rheology*. Vol 1.
19. Simpson MM, Janna WS. Newtonian and non-Newtonian fluids: Velocity profiles, viscosity data, and laminar flow friction factor equations for flow in a circular duct. *ASME Int Mech Eng Congr Expo Proc*. 2009;9(January 2008):173-180. doi:10.1115/IMECE2008-67611
20. Bird GR, Parrish M. The Wire Grid as a Near-Infrared Polarizer. *J Opt Soc Am*. 1960;50(9):886. doi:10.1364/josa.50.000886
21. Reviewed P, Berkeley L, Cancer B. Lawrence Berkeley National Laboratory Lawrence Berkeley National Laboratory. 2010;(July):35-43.
22. Skelland AP. Asymptotic rates of heat or mass transfer in non-newtonian laminar flow. *Ind Eng Chem Fundam*. 1967;6(1):148-151. doi:10.1021/i160021a028
23. Reviews A, Leonard J, Poiseuille M. the History of Poiseuille ' S. *Annu Rev Fluid Mech*. 1953;(25):1-19.
24. Leicester HM. Review Reviewed Work (s): Geschichte der mechanischen Prinzipien und ihrer wichtigsten Anwendungen by István Szabó Review by : E . A . Fellmann Published by : The University of Chicago Press on behalf of The History of Science Society Stable URL : https. 2021;70(3):469-471.
25. Stokes S. *On the Friction of Fluids in Motion, and the Equilibrium and Motion of Elastic Solids*. Vol 8.; 1846. http://www.nawcc-index.net/Articles/Stokes-InternalFriction.pdf
26. Pratima Bajpai. Biermann's Handbook of Pulp and Paper (Third Edition). 2018;Volume 2:455-482. doi:10.1016/B978-0-12-814238-7.00023-4

27. Ostadfar A. *Fluid Mechanics and Biofluids Principles*.; 2016. doi:10.1016/b978-0-12-802408-9.00001-6

28. Mort TC, Keck JP. *Endotracheal Tube and Respiratory Care*. Elsevier Inc.; 2013. doi:10.1016/B978-0-323-22805-3.00009-8

29. Martin S. A hydrodynamic curiosity: The salt oscillator. *Geophys Fluid Dyn*. 1970;1(1-2):143-160. doi:10.1080/03091927009365771

30. Zhang JXJ, Hoshino K. Microfluidics and Micro Total Analytical Systems. *Mol Sensors Nanodevices*. Published online 2014:103-168. doi:10.1016/b978-1-4557-7631-3.00003-x

31. Starosolski Z, Ezon DS, Krishnamurthy R, et al. Soft tissue models: easy and inexpensive flexible 3D printing as a help in surgical planning of cardiovascular disorders. *Med Imaging 2017 Imaging Informatics Heal Res Appl*. 2017;10138(March 2017):101380Q. doi:10.1117/12.2253961

32. Kim NP, Eo JS, Cho D. Optimization of piston type extrusion (PTE) techniques for 3D printed food. *J Food Eng*. 2018;235:41-49. doi:10.1016/j.jfoodeng.2018.04.019

33. Kim NP, Cho D, Zielewski M. Optimization of 3D printing parameters of Screw Type Extrusion (STE) for ceramics using the Taguchi method. *Ceram Int*. 2019;45(2):2351-2360. doi:10.1016/j.ceramint.2018.10.152

34. Sun J, Zhou W, Yan L, Huang D, Lin L ya. Extrusion-based food printing for digitalized food design and nutrition control. *J Food Eng*. 2018;220:1-11. doi:10.1016/j.jfoodeng.2017.02.028

35. Kevin Asthon. That ' Internet of Things ' Thing. *RFID J*. Published online 2010:4986. http://www.rfidjournal.com/article/print/4986

36. Feng Xia, LaurenceT.Yang, Lizhe Wang, Alexey Vinel. Internet of Things. *Int J Commun*

Syst. 2010;23(5):633-652. doi:10.1002/dac.2417

37. Atzori L, Iera A, Morabito G. The Internet of Things: A survey. *Comput Networks*. 2010;54(15):2787-2805. doi:10.1016/j.comnet.2010.05.010

38. Li S, Xu L Da, Zhao S. The internet of things: a survey. *Inf Syst Front*. 2015;17(2):243-259. doi:10.1007/s10796-014-9492-7

39. Jernvall J, Thesleff I. Tooth shape formation and tooth renewal: Evolving with the same signals. *Dev*. 2012;139(19):3487-3497. doi:10.1242/dev.085084

40. Whitlock JA, Richman JM. Biology of tooth replacement in amniotes. *Int J Oral Sci*. 2013;5(2):66-70. doi:10.1038/ijos.2013.36

41. Malmgren B, Andreasen JO, Flores MT, et al. Guidelines for the management of traumatic dental injuries: 3. Injuries in the primary dentition. *Pediatr Dent*. 2017;39(6):420-428. doi:10.1111/j.1600-9657.2012.01146.x

42. Luis Schwab G, Tetu Moysés S, Helena Sottile França B, Iani Werneck R, Frank E, Jorge Moysés S. Chronic conditions policies: Oral health, a felt absence. *Int Dent J*. 2014;64(2):83-88. doi:10.1111/idj.12066

43. Elani HW, Harper S, Thomson WM, et al. Social inequalities in tooth loss: A multinational comparison. *Community Dent Oral Epidemiol*. 2017;45(3):266-274. doi:10.1111/cdoe.12285

44. Sanders AE, Slade GD, Turrell G, Spencer AJ, Marcenes W. Does psychological stress mediate social deprivation in tooth loss? *J Dent Res*. 2007;86(12):1166-1170. doi:10.1177/154405910708601205

45. Bernabé E, Marcenes W. Income inequality and tooth loss in the United States. *J Dent Res*. 2011;90(6):724-729. doi:10.1177/0022034511400081

46. Müller DD, Bissinger R, Reymus M, Bücher K, Hickel R, Kühnisch J. Survival and complication analyses of avulsed and replanted permanent teeth. *Sci Rep*. 2020;10(1):1-9. doi:10.1038/s41598-020-59843-1

47. Mitsiadis TA, Harada H. Regenerated teeth: The future of tooth replacement. An update. *Regen Med*. 2015;10(1):5-8. doi:10.2217/rme.14.78

48. Ikeda E, Morita R, Nakao K, et al. Fully functional bioengineered tooth replacement as an organ replacement therapy. *Proc Natl Acad Sci U S A*. 2009;106(32):13475-13480. doi:10.1073/pnas.0902944106

49. NRC. A History of Dentistry FROM THE MOST ANCIENT TIMES UNTIL THE END OF THE EIGHTEENTH CENTURY. *Oxford Univ*. 1994;XXX:60.

50. Qassadi W, Alshehri T, Alshehri A. Review on Dental Implantology. *Egypt J Hosp Med*. 2018;71(1):2217-2225. doi:10.12816/0045293

51. International Congress of Oral implantologist. Glossary of Implant Dentistry #3. Published online 2017:209.

52. Osman RB, Swain M V. A critical review of dental implant materials with an emphasis on titanium versus zirconia. *Materials (Basel)*. 2015;8(3):932-958. doi:10.3390/ma8030932

53. LEVENTHAL GS. Titanium, a metal for surgery. *J Bone Joint Surg Am*. 1951;33 A(2):473-474. doi:10.2106/00004623-195133020-00021

54. CLARKE EG, HICKMAN J. An investigation into the correlation between the electrical potentials of metals and their behaviour in biological fluids. *J Bone Joint Surg Br*. 1953;35 B(3):467-473. doi:10.1302/0301-620x.35b3.467

55. Albrektsson T, Zarb G, Worthington P, Eriksson AR. The long-term efficacy of currently used dental implants: a review and proposed criteria of success. *Int J Oral Maxillofac*

Implants. 1986;1(1):11-25. http://www.ncbi.nlm.nih.gov/pubmed/3527955

56. Okabe T, Hero H. The use of titanium in dentistry. *Cells Mater*. 1995;5(2):211-230.

57. Zhang Y, Chu K, He S, Wang B, Zhu W, Ren F. Fabrication of high strength, antibacterial and biocompatible Ti-5Mo-5Ag alloy for medical and surgical implant applications. *Mater Sci Eng C*. 2020;106(September 2019):110165. doi:10.1016/j.msec.2019.110165

58. Liu X, Chen S, Tsoi JKH, Matinlinna JP. Binary titanium alloys as dental implant materials-a review. *Regen Biomater*. 2017;4(5):315-323. doi:10.1093/rb/rbx027

59. Buser D, Nydegger T, Oxland T, et al. Interface shear strength of titanium implants with a sandblasted and acid-etched surface: A biomechanical study in the maxilla of miniature pigs. *J Biomed Mater Res*. 1999;45(2):75-83. doi:10.1002/(SICI)1097-4636(199905)45:2<75::AID-JBM1>3.0.CO;2-P

60. Yan Guo C, Tang ATH, Matinlinna JP. Insights into surface treatment methods of titanium dental implants. *J Adhes Sci Technol*. 2012;26(1-3):189-205. doi:10.1163/016942411X569390

61. Le Guéhennec L, Soueidan A, Layrolle P, Amouriq Y. Surface treatments of titanium dental implants for rapid osseointegration. *Dent Mater*. 2007;23(7):844-854. doi:10.1016/j.dental.2006.06.025

62. Přikrylová J, Procházková J, Podzimek Š. Side Effects of Dental Metal Implants: Impact on Human Health (Metal as a Risk Factor of Implantologic Treatment). *Biomed Res Int*. 2019;2019. doi:10.1155/2019/2519205

63. Goutam M, Giriyapura C, Mishra S, Gupta S. Titanium allergy: A literature review. *Indian J Dermatol*. 2014;59(6):630. doi:10.4103/0019-5154.143526

64. Hallab NJ, Mikecz K, Vermes C, Skipor A, Jacobs JJ. Differential lymphocyte reactivity

to serum-derived metal-protein complexes produced from cobalt-based and titanium-based implant alloy degradation. *J Biomed Mater Res*. 2001;56(3):427-436. doi:10.1002/1097-4636(20010905)56:3<427::AID-JBM1112>3.0.CO;2-E

65. Valentine-Thon E, Müller K, Guzzi G, Kreisel S, Ohnsorge P, Sandkamp M. LTT-MELISA® is clinically relevant for detecting and monitoring metal sensitivity. *Neuroendocrinol Lett*. 2006;27(SUPPL. 1):17-24.

66. LeGeros RZ. Calcium phosphate-based osteoinductive materials. *Chem Rev*. 2008;108(11):4742-4753. doi:10.1021/cr800427g

67. Salgado AJ, Coutinho OP, Reis RL. Bone tissue engineering: State of the art and future trends. *Macromol Biosci*. 2004;4(8):743-765. doi:10.1002/mabi.200400026

68. Yin XH, Yan L, Jun Hao D, et al. Calcium alginate template-mineral substituted hydroxyapatite hydrogel coated titanium implant for tibia bone regeneration. *Int J Pharm*. 2020;582(April):119303. doi:10.1016/j.ijpharm.2020.119303

69. Albee FH. Studies in Bone Growth: Triple Calcium Phosphate As a Stimulus To Osteogenesis. *Ann Surg*. 1920;71(1):32-39. doi:10.1097/00000658-192001000-00006

70. LeGeros RZ. Calcium phosphate materials in restorative dentistry: a review. *Adv Dent Res*. 1988;2(1):164-180. doi:10.1177/08959374880020011101

71. Linkow Cesare Brusotti Enrico Cislaghi Pier Luigi Floris Dino Garbaccio Hans Grafelmann Araceli Morales Sánchez Benito Vernole L, titolo CM. Ugo Pasqualini-Marco E. Pasqualini TREATISE OF IMPLANT DENTISTRY.

72. Sierraalta M, Vivas JL, Razzoog ME, Wang RF. Precision of fit of titanium and cast implant frameworks using a new matching formula. *Int J Dent*. 2012;2012. doi:10.1155/2012/374315

73. Stančeková D, Já Š, Martikáň A, Rákoci J, Janota M. Milling of nano-structured bio-materials for dental implants manufacturing. Published online 2015:242-248.

74. Matin KA, Manderson RD. The influence of sprue design on cobalt chromium alloy casting defects. *J Dent*. 1984;12(2):175-182. doi:10.1016/0300-5712(84)90052-6

75. Gouveia PF, Schabbach LM, Souza JCM, et al. New perspectives for recycling dental zirconia waste resulting from CAD/CAM manufacturing process. *J Clean Prod*. 2017;152:454-463. doi:10.1016/j.jclepro.2017.03.117

76. Tunchel S, Blay A, Kolerman R, Mijiritsky E, Shibli JA. 3D Printing/Additive Manufacturing Single Titanium Dental Implants: A Prospective Multicenter Study with 3 Years of Follow-Up. *Int J Dent*. 2016;2016. doi:10.1155/2016/8590971

77. Oliveira TT, Reis AC. Fabrication of dental implants by the additive manufacturing method: A systematic review. *J Prosthet Dent*. 2019;122(3):270-274. doi:10.1016/j.prosdent.2019.01.018

78. Sing SL, An J, Yeong WY, Wiria FE. Laser and electron-beam powder-bed additive manufacturing of metallic implants: A review on processes, materials and designs. *J Orthop Res*. 2016;34(3):369-385. doi:10.1002/jor.23075

79. Irsen SH, Milz S, Tille C, Schieker M, Seitz H. Hydroxyapatite scaffolds for bone tissue engineering made by 3D printing. 2005;6:1121-1124.

80. Suwanprateeb J, Sanngam R, Panyathanmaporn T. Influence of raw powder preparation routes on properties of hydroxyapatite fabricated by 3D printing technique. *Mater Sci Eng C*. 2010;30(4):610-617. doi:10.1016/j.msec.2010.02.014

81. Cox SC, Thornby JA, Gibbons GJ, Williams MA, Mallick KK. 3D printing of porous hydroxyapatite scaffolds intended for use in bone tissue engineering applications. *Mater*

Sci Eng C. 2015;47:237-247. doi:10.1016/j.msec.2014.11.024

82. González Ocampo JI, Escobar Sierra DM, Ossa Orozco CP. Porous bodies of hydroxyapatite produced by a combination of the gel-casting and polymer sponge methods. *J Adv Res*. 2016;7(2):297-304. doi:10.1016/j.jare.2015.06.006

83. Yoshikawa H, Tamai N, Murase T, Myoui A. Interconnected porous hydroxyapatite ceramics for bone tissue engineering. *J R Soc Interface*. 2009;6(SUPPL. 3). doi:10.1098/rsif.2008.0425.focus

84. Tamai N, Myoui A, Tomita T, et al. Novel hydroxyapatite ceramics with an interconnective porous structure exhibit superior osteoconduction in vivo. *J Biomed Mater Res*. 2002;59(1):110-117. doi:10.1002/jbm.1222

85. Nakao K, Morita R, Saji Y, et al. The development of a bioengineered organ germ method. *Nat Methods*. 2007;4(3):227-230. doi:10.1038/nmeth1012

86. Yoshikawa M, Tsuji N, Shimomura Y, Hayashi H, Ohgushi H. Effects of laminin for osteogenesis in porous hydroxyapatite. *Macromol Symp*. 2007;253:172-178. doi:10.1002/masy.200750724

87. Mastrangelo F, Nargi E, Carone L, et al. Tridimensional response of human dental follicular stem cells onto a synthetic hydroxyapatite scaffold. *J Heal Sci*. 2008;54(2):154-161. doi:10.1248/jhs.54.154

88. Jo YY, Lee HJ, Kook SY, et al. Isolation and characterization of postnatal stem cells from human dental tissues. *Tissue Eng*. 2007;13(4):767-773. doi:10.1089/ten.2006.0192

89. Marco Tatullo, Massimo Marrelli, Kevin M. Shakesheff LJW. Dental pulp stem cells: function, isolation and applications in regenerative medicine. *J Tissue Eng Regen Med*. 2015;12(3):181-204. doi:10.1002/term

90. Nuti N, Corallo C, Chan BMF, Ferrari M, Gerami-Naini B. Multipotent Differentiation of Human Dental Pulp Stem Cells: a Literature Review. *Stem Cell Rev Reports*. 2016;12(5):511-523. doi:10.1007/s12015-016-9661-9

91. Lee CH, Hajibandeh J, Suzuki T, Fan A, Shang P, Mao JJ. Three-dimensional printed multiphase scaffolds for regeneration of periodontium complex. *Tissue Eng - Part A*. 2014;20(7-8):1342-1351. doi:10.1089/ten.tea.2013.0386

Vita

Abhilash Aditya was born in Bengaluru, Karnataka, India. Abhilash graduated from JSS Academy of Technical Education in 2012 with Bachelor's Degree in Mechanical Engineering. Abhilash decided to join The University of Texas at El Paso to pursue Master of Science degree in Manufacturing Engineering. Abhilash worked as a graduate research assistant under Dr. Amit J Lopes and then under Dr. Tzu – Liang (Bill) Tseng. His work involved 3D printers, statistical analysis, predictive modeling, and drug delivery systems. After graduating in December 2017, he pursued his post-graduation studies in Material science and Engineering while continuing as a graduate research assistant under the guidance of Dr. Namsoo Peter Kim. His initial research work involved microneedle drug delivery systems with different compatible biopolymers. His interest in additive manufacturing technology made him earn a graduate certificate in 3D engineering and additive manufacturing. Abhilash continued his research on 3D printing of high viscous fluids, an innovative approach of using 3D printers in dental, telemedicine, and food industries. Abhilash has several published works related to his research.

Apart from academics, Abhilash was also involved in student organizations and served as the President of the Indian Student Association (ISA) (2016-17). Abhilash was also a part of the Lombardi Formula SAE team and worked as a designer for the front and rear suspension of the SAE race car. Abhilash was awarded the Anita Mochen Loya Scholarship in 2018. Abhilash also tutored physics, chemistry, and mathematics to undergraduate athletes at Miners Athletic Academic Center (2018-19).

Contact Information:
Abhilash Aditya
aaditya@miners.utep.edu; abhilash91aditya@gmail.com
This dissertation was typed by Abhilash Aditya.